

Distance Scale Zero-Points from Galactic RR Lyrae Star Parallaxes¹

G. Fritz Benedict², Barbara E. McArthur², Michael W. Feast^{3,9}, Thomas G. Barnes²,
Thomas E. Harrison^{4,8}, Jacob L. Bean^{12,17}, John W. Menzies⁹, Brian Chaboyer¹⁶, Luca
Fossati¹³, Nicole Nesvacil^{10,19}, Horace A. Smith⁷, Katrien Kolenberg^{10,12}, C. D. Laney^{9,15},
Oleg Kochukhov¹⁴, Edmund P. Nelan¹¹, D. V. Shulyak¹⁸, Denise Taylor¹¹, Wendy L.
Freedman⁶

ABSTRACT

²McDonald Observatory, University of Texas, Austin, TX 78712

³Centre for Astrophysics, Cosmology and Gravitation, Astronomy Dept, University of Cape Town, Rondebosch, South Africa, 7701

⁴Department of Astronomy, New Mexico State University, Las Cruces, NM 88003

⁵Department of Astronomy, University of Virginia, Charlottesville, VA 22903

⁶The Observatories, Carnegie Institution of Washington, Pasadena, CA 91101

⁷Dept. of Physics & Astronomy, Michigan State University, East Lansing, MI 48824

⁸Visiting Astronomer, Kitt Peak National Observatory, National Optical Astronomy Observatory, which is operated by the Association of Universities for Research in Astronomy, Inc., under cooperative agreement with the National Science Foundation.

⁹South African Astronomical Observatory, Observatory, South Africa, 7935

¹⁰Institute of Astronomy, University of Vienna, A-1180, Vienna, Austria

¹¹STScI, Baltimore MD 21218

¹²Harvard-Smithsonian Center for Astrophysics, Cambridge MA 02138

¹³Department of Physics and Astronomy, Open University, Milton Keynes UK MK7 6AA

¹⁴Department of Physics and Astronomy, Uppsala University, 75120, Uppsala, Sweden

¹⁵Department of Physics and Astronomy, Brigham Young University, Provo, UT 84602

¹⁶Department of Physics and Astronomy, Dartmouth College, Hanover, NH 03755

¹⁷Visiting Astronomer, Cerro-Tololo Inter-American Observatory, which is operated by the Association of Universities for Research in Astronomy, Inc., under cooperative agreement with the National Science Foundation.

¹⁸Institute of Astrophysics, Georg-August-University, Friedrich-Hund-Platz 1, D-37077, Göttingen, Germany

¹⁹Department of Radiotherapy, Medical University of Vienna, A-1090 Vienna, Austria

We present new absolute trigonometric parallaxes and proper motions for seven Pop II variable stars: five RR Lyr variables; RZ Cep, XZ Cyg, SU Dra, RR Lyr, UV Oct; and two type 2 Cepheids; VY Pyx and κ Pav. We obtained these results with astrometric data from Fine Guidance Sensors, white-light interferometers on *Hubble Space Telescope*. We find absolute parallaxes in milliseconds of arc: RZ Cep, 2.12 ± 0.16 mas; XZ Cyg, 1.67 ± 0.17 mas; SU Dra, 1.42 ± 0.16 mas; RR Lyr, 3.77 ± 0.13 mas; UV Oct, 1.71 ± 0.10 mas; VY Pyx, 6.44 ± 0.23 mas; and κ Pav, 5.57 ± 0.28 mas; an average $\sigma_\pi/\pi = 5.4\%$. With these parallaxes we compute absolute magnitudes in V and K bandpasses corrected for interstellar extinction and Lutz-Kelker-Hanson bias. Using these RRL absolute magnitudes, we then derive zero-points for M_V -[Fe/H] and M_K -[Fe/H]-Log P relations. The technique of reduced parallaxes corroborates these results. We employ our new results to determine distances and ages of several Galactic globular clusters and the distance of the LMC. The latter is close to that previously derived from Classical Cepheids uncorrected for any metallicity effect, indicating that any such effect is small. We also discuss the somewhat puzzling results obtained for our two type 2 Cepheids.

Subject headings: astrometry — interferometry — stars: distances — stars: individual (κ Pav, VY Pyx, RZ Cep, XZ Cyg, SU Dra, RR Lyr, UV Oct) — distance scale calibration — stars: Cepheids — stars: RR Lyrae variables — galaxies: individual (Large Magellanic Cloud)

1. Introduction

RR Lyrae variable stars (RRL) have long played a crucial role in understanding old stellar populations (Pop II). Paraphrasing Smith (1995), they are important as tracers of the chemical and dynamical properties of old populations, as standard candles in our own and nearby galaxies, and as a test bed for the understanding of stellar pulsation and evolution. Their luminosities are of great potential importance in estimating the distances and hence the ages of globular clusters –both the absolute ages and the relative ages as a function of metallicity, [Fe/H]. An error in distance modulus of 0.1 magnitude corresponds to an age

¹Based on observations made with the NASA/ESA Hubble Space Telescope, obtained at the Space Telescope Science Institute, which is operated by the Association of Universities for Research in Astronomy, Inc., under NASA contract NAS5-26555

uncertainty of 1 Gyr. The RRL are also vital for studies of the structure and formation of our Galaxy, Local Group members and other nearby galaxies, a field which is currently referred to as Near-Field Cosmology. Their importance as distance indicators comes from the fact that they follow $M(V)$ - $[Fe/H]$ and K - $\log P$ or K - $[Fe/H]$ - $\log P$ relations. The zero points of these relations have been much discussed. Trigonometric parallaxes remain the only fundamental method of getting RRL distances and luminosities, free of the assumptions which go into other methods discussed in Section 6.3 below. Absolute parallaxes allow these assumptions to be tested. What is required is an improved fundamental zero-point calibration, which currently rests on the *HST* parallax (Benedict et al. 2002b) of RR Lyrae alone (c.f. Sollima *et al.* 2006). In this paper we apply the astrometric precision of *HST*/FGS to the determination of absolute parallaxes for five galactic RRL: XZ Cyg = Hip 96112; UV Oct = Hip 80990; RZ Cep = Hip 111839; SU Dra = Hip 56734; RR Lyr = Hip 95497; and two type 2 Cepheids, κ Pav = Hip 93015 and VY Pyx = Hip 43736. Target properties are given in Table 1 and discussed in Section 2.

Type 2 Cepheids (hereafter CP2), more luminous than the RR Lyraes, have great potential as distance indicators in old populations. They have recently been shown to define a narrow K-band Period-Luminosity Relation (Matsunaga *et al.* 2006, 2009) with little metallicity dependence. The slope and zero-point of this relation are indistinguishable from that of the RRL derived by Sollima *et al.* (2006). Two CP2, κ Pavonis and VY Pyxidis (confirmed as such by Zakrzewski *et al.* 2000), were expected to be sufficiently close that very accurate parallaxes and absolute magnitudes could be obtained with *HST*. Not only could these parallaxes, likely a factor of three more precise than from *HIPPARCOS*, provide an accurate zero-point for the CP2 Period-Luminosity Relation (PLR), but they may facilitate the derivation of the slope and zero-point of a combined RRL and CP2 PLR. Majaess (2010) has recently asserted that CP2 and RRL define a single-slope PLR when a Wesenheit magnitude, $W_{VI}=V-2.45(V-I)$ is plotted against $\log P$.

In the following sections we describe our astrometry using one of our targets, κ Pav, as an example throughout. This longest-period member of our sample has been identified as a peculiar W Vir star (Feast et al. 2008) but, if included, could anchor our K-band PLR slope. Hence, its parallax value deserves as much external scrutiny as possible. We discuss (Section 2) data acquisition and analysis; present the results of spectrophotometry of the astrometric reference stars required to correct our relative parallax to absolute (Section 3); derive absolute parallaxes for these variable stars (Section 4); derive absolute magnitudes (Section 5); determine (Section 6) a K-band PLR zero point and an M_V - $[Fe/H]$ relation zero point, and compare our resulting absolute magnitudes with past determinations; in Section 7 discuss the distance scale ramifications of our results, and apply our PLR zero points to two interesting classes of object - Globular Clusters (M3, M4, M15, M68, ω Cen, and M92) and

the LMC. In Section 8 we discuss the puzzling results for VY Pyx and κ Pav. We summarize our findings in Section 9.

2. Observations and Data Reduction

Nelan (2010) provides an overview of the Fine Guidance Sensor (FGS) instrument (a two-axis shearing interferometer), and Benedict et al. (2007) describe the fringe tracking (POS) mode astrometric capabilities of an FGS, along with the data acquisition and reduction strategies also used in the present study. We time-tag our data with a modified Julian Date, $\text{MJD} = \text{JD} - 2400000.5$.

Between thirteen and twenty-three sets of astrometric data were acquired with *HST* FGS 1r for each of our seven science targets. We obtained most of these sets at epochs determined by field availability, primarily dictated by two-gyro guiding constraints. See Benedict et al. (2010) for a brief discussion of these constraints. The various complete data aggregates span from 2.37 to 13.14 years. Table 2 contains the epochs of observation, pulsational phase, the V magnitude, and estimated B-V color index (required for the lateral color correction discussed in Section 4.1) for each variable. The B-V colors are inferred from phased color curves constructed from various sources: XZ Cyg (Sturch 1966); RZ Cep (Epps & Sinclair 1973); SU Dra (Barcza 2002); RR Lyr (Hardie 1955); UV Oct (Kolenberg, private comm.); κ Pav (Shobbrook 1992); VY Pyx (Sanwal & Sarma 1991).

Each individual *HST* data set required approximately 33 minutes of spacecraft time. The data were reduced and calibrated as detailed in McArthur et al. (2001), Benedict et al. (2002a), Benedict et al. (2002b), Soderblom et al. (2005), and Benedict et al. (2007). At each epoch we measured reference stars and the target multiple times to correct for intra-orbit drift of the type seen in the cross filter calibration data shown in figure 1 of Benedict et al. (2002a). The distribution of reference stars on a second generation Digital Sky Survey R image near each of our science targets is shown in Figure 1. The orientation of each successive observation changes, mandated by *HST* solar panel illumination constraints.

Data are downloaded from the *HST* archive and passed through a pipeline processing system. This pipeline extracts the astrometry measurements (typically one to two minutes of fringe x and y position information acquired at a 40 Hz rate, which yields several thousand discrete measurements), extracts the median (which we have found to be the optimum estimator of position), corrects for the Optical Field Angle Distortion (McArthur et al. 2002), and attaches all required time tags and parallax factors.

Table 1 collects measured properties for our target variables, including stellar type

(ab or c for RRL), log of the pulsational period, $\langle V \rangle$, $\langle K \rangle$, $\langle B-V \rangle$, $E(B-V)$, A_V , and A_K . Photometry is from the various sources noted in the table. The $\langle K \rangle$ is in the 2MASS system. All reddening values are adopted from those listed in Fernley et al. (1998a) or Feast et al. (2008) with a sanity check provided by our reference star photometry.

Our default metallicity source is Fernley et al. (1998a). The metallicity of RR Lyr is from Kolenberg et al. (2010). The metallicities of UV Oct and VY Pyx were determined for this paper, using the approach described in Kolenberg et al. (2010), determined by analysis of Fe line equivalent widths measured from high-resolution spectra. The κ Pav metallicity is from Luck & Bond (1989). The Fernley et al. (1998a) metallicities agree with Layden (1994) for the brighter stars in common ($V < 11$). Because the Layden (1994) metallicities are on the ZW (Zinn & West 1984) scale we assume the same scale for the Fernley et al. (1998a) metallicities. Because the Kolenberg et al. (2010) RR Lyrae metallicity agrees with Fernley et al. (1998a), we presume that it too is ZW. Therefore we believe our metallicities are on, or close to, the ZW scale. This is the scale we use to establish zero-points that will be applied later to derive distances.

Finally, three stars in our sample (including RR Lyrae) exhibit Blazhko cycles, wherein the maximum and minimum brightness vary over time. Smith and Kolenberg have studied this phenomenon for many such stars (see, e.g., LaCluyze et al. 2004, Kolenberg et al. 2006, 2010, Blazhko Project website <http://www.univie.ac.at/tops/blazhko/>) and conclude from recent data that the total output of the target Blazhko stars averaged over a cycle remains constant within 0.03 mag, in accordance with the findings by Alcock et al. (2003). As the peak brightness decreases, the minimum brightness increases. Blazhko is not a disease that renders RRL poor standard candles as further demonstrated in Cacciari et al. (2005).

3. Spectrophotometric Parallaxes of the Astrometric Reference Stars

The following review of our astrometric and spectrophotometric techniques uses the κ Pav field as an example. Because the parallaxes determined for the variables will be measured with respect to reference frame stars which have their own parallaxes, we must either apply a statistically derived correction from relative to absolute parallax (Van Altena, Lee & Hoffleit 1995, hereafter YPC95) or estimate the absolute parallaxes of the reference frame stars. In principle, the colors, spectral type, and luminosity class of a star can be used to estimate the absolute magnitude, M_V , and V-band absorption, A_V . The absolute parallax is then simply,

$$\pi_{abs} = 10^{\frac{-(V - M_V + 5 - A_V)}{5}} \quad (1)$$

The luminosity class is generally more difficult to estimate than the spectral type (tem-

perature class). However, the derived absolute magnitudes are critically dependent on the luminosity class. As a consequence we use as much additional information as possible in an attempt to confirm the luminosity classes. Specifically, we obtain 2MASS¹ photometry and proper motions from the PPMXL catalog (Roeser et al. 2010) for a one degree square field centered on each science target, and iteratively employ the technique of reduced proper motion (Yong & Lambert 2003, Gould & Morgan 2003) to confirm our giant/dwarf classifications (Section 4.2).

3.1. Reference Star Photometry

Our band passes for reference star photometry include: BV from recent measurements with the New Mexico State University 1m telescope (Holtzman et al. 2010) for RR Lyr, SU Dra, XZ Cyg, and RZ Cep fields; from the South African Astronomical Observatory (SAAO) 1m for the UV Oct, κ Pav and VY Pyx fields; from the SMARTS 0.9m (Subasavage et al. 2010) for the VY Pyx and UV Oct fields; and JHK (from 2MASS). Table 3 lists BVJHK photometry for our reference stars bright enough to have 2MASS measurements.

3.2. Reference Star Spectroscopy

Spectral classifications for reference stars in the UV Oct, κ Pav and VY Pyx fields were provided by the South African Astronomical Observatory (SAAO) 1.9m telescope. The SAAO resolution was 3.5 Å/ (FWHM) with wavelength coverage from $3750 \text{ Å} \leq \lambda \leq 5500 \text{ Å}$. Spectroscopic classification of the reference stars in the fields of RR Lyr, SU Dra, XZ Cyg, and RZ Cep was accomplished using data obtained with the Double Imaging Spectrograph (DIS) on the Apache Point Observatory 3.5 m telescope². We used the high-resolution gratings, delivering a dispersion of 0.62 Å/pix, and covering the wavelength range of $3864 \leq \lambda \leq 5158 \text{ Å}$. Spectroscopy of the reference stars in the fields of UV Oct, κ Pav and VY Pyx was also obtained using the RC Spectrograph on the CTIO Blanco 4 m. The Loral3K CCD detector with KPGL1-1 grating was used to deliver a dispersion of 1.0 Å/pix, covering the wavelength range $3500 \leq \lambda \leq 5830 \text{ Å}$. Classifications used a combination of template matching and line ratios. Spectral types for the stars are generally better than ± 2 subclasses.

¹The Two Micron All Sky Survey is a joint project of the University of Massachusetts and the Infrared Processing and Analysis Center/California Institute of Technology

²The Apache Point Observatory 3.5 m telescope is owned and operated by the Astrophysical Research Consortium.

3.3. Interstellar Extinction

To determine interstellar extinction we first plot the reference stars on a J-K vs. V-K color-color diagram. A comparison of the relationships between spectral type and intrinsic color against those we measured provides an estimate of reddening. Figure 2 contains the κ Pav J-K vs V-K color-color diagram and reddening vector for $A_V = 1.0$. Also plotted are mappings between spectral type and luminosity class V and III from Bessell & Brett (1988) and Cox (2000). Figure 2, along with the estimated spectral types, provides an indication of the reddening for each reference star.

Assuming an $R = 3.1$ Galactic reddening law (Savage & Mathis 1979), we derive A_V values by comparing the measured colors (Table 3) with intrinsic $(V-K)_0$ and $(B-V)_0$ colors from Cox (2000). We estimate A_V from $A_V = 1.1E(V-K) = 3.1E(B-V)$, where the ratios of total to selective extinction were derived from the Savage & Mathis (1979) reddening law and a reddening estimate in the direction of κ Pav from Schlegel et al. (1998), via NED³. All resulting A_V are collected in Table 4. These are the A_V used in Equation 1.

Using the κ Pav field as an example, we find that the technique of reduced proper motions can provide a possible confirmation of reference star estimated luminosity classes. The precision of existing proper motions for all the reference stars is $\sim 5 \text{ mas y}^{-1}$, only suggesting discrimination between giants and dwarfs. Typical errors on H_K , a parameter equivalent to absolute magnitude, M , were about a magnitude. Nonetheless, a reduced proper motion diagram did suggest that ref-31 is not a dwarf star. Our luminosity class uncertainty is reflected in the input spectrophotometric parallax errors (Table 4). We will revisit this additional test in Section 4.2, once we have higher precision proper motions obtained from our modeling.

3.4. Estimated Reference Frame Absolute Parallaxes

We derive absolute parallaxes for each reference star using M_V values as a function of spectral type and luminosity class from Cox (2000) and the A_V derived from the photometry. Our adopted errors for $(m-M)_0$ are 0.5 mag for all reference stars. This error includes uncertainties in A_V and the spectral types used to estimate M_V . Our reference star parallax estimations from Equation 1 are listed in Table 4. Similar data for the RR Lyr reference frame can be found in Benedict et al. (2002b). For the κ Pav field individually, no reference star absolute parallax is better determined than $\frac{\sigma_\pi}{\pi} = 23\%$. The average absolute parallax

³NASA/IPAC Extragalactic Database

for the reference frame is $\langle\pi_{abs}\rangle = 1.5$ mas. We compare this to the correction to absolute parallax discussed and presented in YPC95. Entering YPC95, section 3.2, fig. 2, with the κ Pav Galactic latitude, $\ell = -25^\circ$, and average magnitude for the reference frame, $\langle V_{ref} \rangle = 14.2$, we obtain a correction to absolute of 1.2 mas. This gives us confidence in our spectrophotometric determination of the correction to absolute parallax. As in past investigations we prefer to introduce into our reduction model our spectrophotometrically estimated reference star parallaxes as observations with error. The use of spectrophotometric parallaxes offers a more direct (less Galaxy model-dependent) way of determining the reference star absolute parallaxes.

4. Absolute Parallaxes of Population II Variable Stars

4.1. The Astrometric Model

With the positions measured by FGS 1r (and FGS 3 for RR Lyr) we determine the scale, rotation, and offset “plate constants” relative to an arbitrarily adopted constraint epoch (the so-called “master plate”) for each observation set (the data acquired at each epoch). The MJD of each observation set is listed in Table 2, along with a measured magnitude transformed from the FGS instrumental system as per Benedict *et al.* (1998), but with coefficients determined for FGS 1r. Our κ Pav reference frame contains 6 stars. Several primary science targets (RR Lyr, VY Pyx, and κ Pav) are bright enough to require the use of the FGS neutral density filter. For those objects we use the modeling approach outlined in Benedict *et al.* (2002b), with corrections for both cross-filter and lateral color positional shifts, using values specific to FGS 1r or FGS 3 determined from previous calibration observations with each FGS.

We employ GaussFit (Jefferys *et al.* 1988) to minimize χ^2 . The solved equations of condition for the κ Pav field are:

$$x' = x + lc_x(B - V) - \Delta XF_x \quad (2)$$

$$y' = y + lc_y(B - V) - \Delta XF_y \quad (3)$$

$$\xi = Ax' + By' + C - \mu_x \Delta t - P_\alpha \pi_x \quad (4)$$

$$\eta = -Bx' + Ay' + F - \mu_y \Delta t - P_\delta \pi_y \quad (5)$$

where x and y are the measured coordinates from *HST*; lc_x and lc_y are the lateral color corrections; ΔXF_x and ΔXF_y are the cross filter corrections in x and y , applied only to the observations of RR Lyr and the CP2; and $B - V$ are the B-V colors of each star. A and B

are scale and rotation plate constants, C and F are offsets; μ_x and μ_y are proper motions; Δt is the epoch difference from the mean epoch; P_α and P_δ are parallax factors; and π_x and π_y are the parallaxes in x and y. We obtain the parallax factors from a JPL Earth orbit predictor (Standish 1990), upgraded to version DE405.

4.2. Prior Knowledge and Modeling Constraints

In a quasi-Bayesian approach the reference star spectrophotometric absolute parallaxes (Table 4) and PPMXL proper motions (Table 6) were input as observations with associated errors, not as hardwired quantities known to infinite precision. Input proper motion values have typical errors of 4–6 mas y^{-1} for each coordinate. The lateral color and cross-filter calibrations and the B-V color indices are also treated as observations with error. Proper motion values obtained from our modeling of *HST* data for the κ Pav field are listed in Table 6. Transverse velocities for κ Pav and all our other science targets, given our final parallaxes, are listed below. We employ the technique of reduced proper motions to provide a confirmation of all reference star estimated luminosity classes listed in Table 4. We obtain proper motion and J, K photometry from PPMXL and 2MASS for a $\frac{1}{3}^\circ \times \frac{1}{3}^\circ$ field centered on all RRL and CP2. Figure 3 shows $H_K = K + 5\log(\mu)$ plotted against J-K color index for 4039 stars. If all stars had the same transverse velocities, Figure 3 would be equivalent to an HR diagram. The RRL, CP2, and associated reference stars are plotted as ID numbers from Table 6. With our now measured, more precise proper motions (Table 6) errors in H_K are now ~ 0.3 magnitude. Note the clumping of the RRL towards the ‘faint’ end of the diagram. Reduced proper motion diagrams are ‘fooled’ by the relatively high space velocities of these halo component giant stars.

We stress that for no CP2 or RRL in our program was a previously measured parallax used as prior knowledge and entered as an observation with error. Only reference star parallax prior knowledge was so employed. Our parallax results are blind to previous RRL and CP2 parallax measures from *Hipparcos* and/or parallaxes from surface brightness estimates.

4.3. Assessing Reference Frame Residuals

The Optical Field Angle Distortion calibration (McArthur *et al.* 2002) reduces as-built *HST* telescope and FGS 1r distortions with amplitude $\sim 1''$ to below 2 mas over much of the FGS 1r field of regard. From histograms of the κ Pav field astrometric residuals (Figure 4) we conclude that we have obtained satisfactory correction. The resulting reference frame

‘catalog’ in ξ and η standard coordinates (Table 5) was determined with average position errors $\langle\sigma_\xi\rangle = 0.46$ and $\langle\sigma_\eta\rangle = 0.46$ mas.

To determine if there might be unmodeled - but possibly correctable - systematic effects at the 1 mas level, we plotted reference frame X and Y residuals against a number of spacecraft, instrumental, and astronomical parameters. These included X, Y position within our total field of view; radial distance from the field of view center; reference star V magnitude and B-V color; and epoch of observation. We saw no obvious trends.

4.3.1. The Absolute Parallax of κ Pav

We constrain $\pi_x = \pi_y$ in Equations 3, 4 and obtain for κ Pav a final absolute parallax $\pi_{abs} = 5.57 \pm 0.28$ mas. We have achieved a significant reduction in formal error, with the HIP97 determination, $\pi_{abs} = 6.00 \pm 0.67$ mas and the HIP07 determination, $\pi_{abs} = 6.52 \pm 0.77$ mas. A surface brightness (pulsation) parallax for κ Pav was determined by Feast et al. (2008) to be 4.90 ± 0.17 mas. The parallax of κ Pav derived in the present work is in better agreement with the pulsation parallax of Feast et al. (2008) (a two sigma difference) than the HIP97 and HIP07 parallaxes. We note that this object is another for which the HIP07 re-reduction has not improved agreement with *HST*. See Barnes (2009) for a few other examples involving galactic Cepheids. Parallaxes and relative proper motion results for all RRL and CP2 are collected in Tables 8 and 7.

4.3.2. Modeling Notes on the RRL and VY Pyx

Final model selection for all fields was based on reference star placement relative to the target, total number of reference stars, reduced χ^2 (χ^2/DOF , where DOF = degrees of freedom), and parallax error. For all but the κ Pav, RR Lyr, and RZ Cep fields we increased the number of modeling coefficients in Equations 3 and 4 to six. We introduced radial terms, resulting in these equations of condition

$$\xi = Ax' + By' + G(x'^2 + y'^2)^{1/2} + C - \mu_x \Delta t - P_\alpha \pi_x \quad (6)$$

$$\eta = -Bx' + Ay' + H(x'^2 + y'^2)^{1/2} + F - \mu_y \Delta t - P_\delta \pi_y \quad (7)$$

Absolute parallaxes, relative proper motions, and transverse velocities for κ Pav and associated reference stars are collected in Table 6. Parallaxes for all RRL and CP2 are collected in Tables 8 and 7.

All our absolute parallaxes directly rely on the estimates of reference star parallaxes. Should anyone wish to verify our results independently, the reference stars used in this study are all identified in archival material⁴ held at the Space Telescope Science Institute. Adopted reference star spectral types for all fields are listed in Table 4.

XZ Cyg - Reference star 2 was removed from the data set because of high and unmodelable residuals. Application of Equations 6,7 to the remaining data resulted in a positional catalog with $\langle\sigma_\xi\rangle = 0.28$ and $\langle\sigma_\eta\rangle = 0.29$ mas. Residuals histograms are well-modeled with Gaussians of dispersion $\sigma_x = 1.4$ mas and $\sigma_y = 1.1$ mas. The resulting parallax, $\pi_{abs} = 1.67 \pm 0.17$ mas, agrees within the far larger errors of either the HIP97 or HIP07 value, $\pi_{abs} = 2.29 \pm 0.85$ mas.

UV Oct - Application of Equations 6,7 to these data resulted in a positional catalog with $\langle\sigma_\xi\rangle = 0.19$ and $\langle\sigma_\eta\rangle = 0.18$ mas. Residuals histograms are well-modeled with Gaussians of dispersion $\sigma_x = 1.0$ mas and $\sigma_y = 0.8$ mas. The resulting parallax, $\pi_{abs} = 1.71 \pm 0.10$ mas is between the HIP97 ($\pi_{abs} = 1.48 \pm 0.94$ mas) or HIP07 ($\pi_{abs} = 2.44 \pm 0.81$ mas) values.

RZ Cep - Reference star 20 was removed from the data set because of high residuals. Application of Equations 4,5 to these data resulted in a positional catalog with $\langle\sigma_\xi\rangle = 0.37$ and $\langle\sigma_\eta\rangle = 0.37$ mas. Residuals histograms are well-modeled with Gaussians of dispersion $\sigma_x = 1.7$ mas and $\sigma_y = 1.2$ mas. The resulting parallax, $\pi_{abs} = 2.54 \pm 0.19$ mas differs from the HIP97 ($\pi_{abs} = 0.22 \pm 1.09$ mas) or HIP07 ($\pi_{abs} = 0.59 \pm 1.48$ mas) values. The *HST* value has a far smaller error.

SU Dra - Reference star 27 was removed from consideration because of high residuals. Application of Equations 6,7 to these data resulted in a positional catalog with $\langle\sigma_\xi\rangle = 0.34$ and $\langle\sigma_\eta\rangle = 0.39$ mas. Residuals histograms have Gaussians with dispersion $\sigma_x = 0.9$ mas and $\sigma_y = 1.0$ mas. The resulting parallax, $\pi_{abs} = 1.42 \pm 0.16$ mas agrees within the larger errors of both HIP97 ($\pi_{abs} = 1.11 \pm 1.09$ mas) and HIP07 ($\pi_{abs} = 0.20 \pm 1.13$ mas), but is far more statistically significant.

RR Lyr - Because temporary onboard science-side failures left *HST* with few operational science instruments in late 2008, we were granted additional orbits for FGS astrometry. One of our targets was RR Lyr, a field for which we obtained five additional orbits. Application of Equations 4,5 to our original FGS 3 and these new data resulted in a positional catalog with $\langle\sigma_\xi\rangle = 0.34$ and $\langle\sigma_\eta\rangle = 0.52$ mas. Residuals histograms are well-fit with Gaussians of dispersion $\sigma_x = 0.7$ mas and $\sigma_y = 0.7$ mas. The resulting parallax, $\pi_{abs} = 3.77 \pm 0.13$ mas is between the HIP97 ($\pi_{abs} = 4.38 \pm 0.59$ mas) or HIP07 ($\pi_{abs} = 3.46 \pm 0.64$ mas) values. Our

⁴<http://www.stsci.edu/observing/phase2-public/11211.pro>

previous parallax value (Benedict et al. 2002b) was $\pi_{abs} = 3.82 \pm 0.20$ mas. The additional *HST* data have significantly improved the parallax and proper motion precision compared to the 2002 values.

VY Pyx - Application of Equations 4,5 to these data resulted in a positional catalog with $\langle\sigma_{\xi}\rangle = 0.23$ and $\langle\sigma_{\eta}\rangle = 0.22$ mas. Residuals histograms are well-modeled with Gaussians of dispersion $\sigma_x = 1.4$ mas and $\sigma_y = 1.0$ mas. The resulting parallax, $\pi_{abs} = 6.44 \pm 0.23$ mas is larger than either the HIP97 ($\pi_{abs} = 5.74 \pm 0.76$ mas) or HIP07 ($\pi_{abs} = 5.01 \pm 0.44$ mas) values. We assessed the residuals from our modeling for evidence of orbital motion that could impact a parallax determination and found no significant signals. As done for all our modeling, we tested each spectrophotometrically determined reference star parallax by solving for a trigonometric parallax relative to the aggregate of reference stars and found no significant departures from the initial estimates. One last potential impact on a final parallax would be inadequate sampling of the parallactic ellipse. We show in Figure 5 the parallax factor coverage for both VY Pyx and RR Lyr. We are confident that our parallax is not affected by poor sampling of the parallactic ellipse of VY Pyx. We shall discuss this parallax result later in Section 5 when we determine absolute magnitudes and in Section 8, wherein we discuss both these peculiar CP2.

4.4. *HST* Parallax Accuracy

Our parallax precision, an indication of our internal, random error, is ~ 0.2 mas. To assess our accuracy, or external error, we have compared (Benedict *et al.* 2002b, Soderblom *et al.* 2005) our parallaxes with results from independent measurements from *HIPPARCOS* (Perryman *et al.* 1997). See McArthur et al. (2011) for a more recent comparison with the *HIPPARCOS* re-reduction of van Leeuwen (2007). Other than for the Pleiades (Soderblom *et al.* 2005), we have no large systematic differences with *HIPPARCOS* for any objects with $\frac{\sigma_{\pi}}{\pi} < 10\%$. The next significant improvement in geometrical parallaxes for Pop II variable stars will come from the space-based, all-sky astrometry missions *Gaia* (Lindegren et al. 2008) with ~ 20 μ arcsec precision parallaxes. Final results are expected early in the next decade.

5. The Absolute Magnitudes of the RRL and CP2

In using measured quantities involving distance, care has to be taken of bias questions. Lutz & Kelker (1973) in a well known paper used a frequentist argument to show that

if stars of the same measured parallax are grouped together, the derived mean parallax will be overestimated. This is because for most Galactic stellar distributions, the stars with overestimated parallaxes will outnumber those with underestimated parallaxes. This argument can be applied to single stars chosen by parallax and the argument can be put in a Bayesian form (see for example section 5 of Benedict et al. 2007). There have been extensive discussions of the method in the literature (see e.g. Smith 2003). Here we have used the general formulation of Hanson (1979) as applied to the determination of absolute magnitudes. This Lutz-Kelker-Hanson (LKH) bias in absolute magnitude is proportional to $(\sigma_\pi/\pi)^2$. Presuming that all RRL and CP2 in Table 2 belong to the same class of object (evolved Pop II stars), we scale the LKH correction determined in Benedict et al. (2002b) for RR Lyr and obtain the LKH bias corrections listed in Tables 8 and 7. The average LKH bias correction for all objects in this study is -0.047 magnitude. We identify the choice of prior for this bias correction as a possible contributor to systematic errors in the zero-points of our PLR at the 0.01 magnitude level. For our example target, κ Pav, we find LKH = -0.02 magnitude (Table 7). We have used these corrected absolute magnitudes in deriving zero-points of the relations discussed below. In addition we have used the uncorrected parallaxes to derive these zero-points by the method of reduced parallaxes (RP). This RP approach avoids some of the bias problems (see Feast 2002 whose general scheme we use).

5.1. An Absolute Magnitude for κ Pav

With $\langle V \rangle = 2.78$ (Table 1) and given the absolute parallax, 5.57 ± 0.28 mas from Section 4.3.1, we determine a distance modulus for κ Pav. For all objects (except RZ Cep, where we adopt the Fernley et al. 1998 value) we adopt a color excess from Feast et al. (2008), which for κ Pav (and an adopted $R = \frac{A_V}{E(B-V)} = 3.1$) yields $\langle A_V \rangle = 0.05$. With this $\langle A_V \rangle$, the measured distance to κ Pav, and the LKH correction we obtain $M_V = -1.99 \pm 0.11$ and a corrected true distance modulus, $(m-M)_0 = 6.29$. From the value in Feast et al. (2008), $\langle K_s \rangle = 2.78$ we obtain $M_K = -3.52 \pm 0.11$.

κ Pav has been identified to be a peculiar W Vir star (Feast et al. 2008; Feast 2010). See Section 8 for additional discussion. Results, including all proper motions and absorption- and LKH bias-corrected absolute magnitudes, for the objects in our program are collected for the CP2 in Table 7 and for the RRL in Table 8.

6. Zero-points for the RRL Period-Luminosity and M_V - Metallicity Relations

6.1. The RRL M_K - $\log P$ Relation

A relation between K and $\log P$ for RRL was found by Longmore et al. (1986) in globular clusters. In more recent times a number of such relations have been suggested and these are given in Equations 8-13, where the zero-points a_n refer to the mean period and metallicity of our parallax sample. The $\log P$ of RZ Cep, an overtone type ‘c’ RRL, has been ‘fundamentalized’ by adding +0.127, a factor determined by comparing type ab and type c RRL, e.g. Ooster et al. (2006). Equation 8 was obtained by Sollima (2008) from globular clusters with distance based on subdwarf parallaxes. Since the metallicity term is small we also give the equation without the metallicity term (Equation 9). Equation 10 is a semi-theoretical derivation. Equation 11 is from RRL in the cluster Reticulum in the LMC. Equation 12 was derived from RRLs of different metallicities in the globular cluster ω Cen, and Equation 13 is from RRL in the field of the LMC. For these relations the metallicities are all on, or close to the Zinn-West system, except Equation 8 where they are on the Carretta-Gratton system. The relations between different systems provided by Carretta & Gratton (1997) show that our mean ZW metallicity (-1.58) converts to -1.40 on the CG scale, and in view of the small size of the metallicity coefficient in Equation 8 the effect is negligible (~ 0.01 mag).

The values of a_n for these equations are listed in Table 9. Two values are given for each equation, one derived by fitting the LKH corrected absolute magnitudes to the equation, and one derived using the method of reduced parallaxes (RP). The difference in the two zero-points are within the uncertainties. Figure 6 shows a K - $\log P$ plot for our data. A slope of -2.38 (Equation 9) was adopted for the fitted line. The CP2 κ Pav, included in the plot, will be discussed below (Section 8). It is not included in the fit.

The various PLR relationships and their sources are:

$$M_K = (-2.38 \pm 0.04)(\log P + 0.28) + (0.08 \pm 0.11)([Fe/H] + 1.58) + a_1, \text{ Sollima et al. 2008} \quad (8)$$

$$M_K = (-2.38 \pm 0.04)(\log P + 0.28) + a_2, \text{ Sollima et al. 2006, neglecting metallicity} \quad (9)$$

$$M_K = -2.101(\log P + 0.28) + (0.231 \pm 0.012)([Fe/H] + 1.58) + a_3, \text{ Bono et al. 2003} \quad (10)$$

$$M_K = (-2.16 \pm 0.09)(\log P + 0.28) + a_4, \text{ Dall'Ora et al. 2004} \quad (11)$$

$$M_K = (-2.71 \pm 0.12)(\log P + 0.28) + (0.12 \pm 0.04)([Fe/H] + 1.58) + a_5, \text{ Del Principe et al. 2006} \quad (12)$$

$$M_K = (-2.11 \pm 0.17)(\log P + 0.28) + (0.05 \pm 0.07)([Fe/H] + 1.58) + a_6, \text{ Borissova et al. 2009} \quad (13)$$

6.2. An RRL M_V - $[\text{Fe}/\text{H}]$ Relation Zero-Point from *HST* Parallaxes

There is a long history of attempts to determine how M_V depends on $[\text{Fe}/\text{H}]$. A linear relation is generally assumed. Our data hint at a slope with the more metal-poor stars brighter. The best estimate for the slope (b) is probably from the work of Gratton et al. (2004), using RRL in the LMC ($b = 0.214$), and we have adopt that slope here. Figure 7 presents our M_V plotted against metallicity, $[\text{Fe}/\text{H}]$, where the metallicity measures are from the sources noted in Table 1, all on the ZW scale. Fitting the function (Gratton et al. 2004)

$$M_V = (0.214 \pm 0.047)([Fe/H] + 1.5) + a_7 \quad (14)$$

to all RRL, we obtain a zero-point, $a_7 = +0.45 \pm 0.05$, listed in Table 9. Hence, $M_V = +0.45 \pm 0.05$ for RRL with $[\text{Fe}/\text{H}] = -1.50$. The regression was carried out using GaussFit (Jefferys et al. 1988), which takes into account uncertainties along both axes. The RMS of this fit, 0.08 mag in M_V , suggests an upper limit on the V-band cosmic dispersion in the absolute magnitudes of RRL. An RP approach finds $M_V = +0.46 \pm 0.03$. Note that the mean metallicity of our five RRL, $\langle [\text{Fe}/\text{H}] \rangle = -1.58$, is so close to -1.50, that the error in the slope makes no significant difference to the zero-point. Bono et al. (2007) find for field RRL a quadratic expression relating M_V to $[\text{Fe}/\text{H}]$; $M_V \propto 0.50[\text{Fe}/\text{H}] + 0.09[\text{Fe}/\text{H}]^2$. We fit (again with GaussFit) the distribution seen in Figure 7, constraining the $[\text{Fe}/\text{H}]$ coefficients to the Bono *et al.* values and find a zero-point $a = 0.98 \pm 0.05$. This and our average $\langle [\text{Fe}/\text{H}] \rangle = -1.58$ yields $\langle M_V \rangle = 0.42$, consistent with the Gratton et al. (2004) parameterization.

Regarding the intrinsic dispersion in RRL absolute magnitudes due to evolutionary effects, the intrinsic width of the RRL distribution in GC near this metallicity has been shown by Sandage (1990) to be ± 0.2 mag. Thus the standard deviation of a uniformly filled strip is 0.057. For five stars, the standard error we would find given such a strip (absent observational uncertainty) is 0.029 mag. Our observational uncertainty standard error for the five is 0.024 mag. Combine the two in quadrature and our claim of ± 0.05 mag is actually a bit conservative.

6.3. Comparison with Previous Determinations of RRL M_V and M_K

We compare in Table 10 past determinations of RRL M_V with our new value, $M_V = +0.45 \pm 0.05$ from LKH and $M_V = +0.46 \pm 0.03$ from the RP determination. An historical summary to the early 1990s is given by Smith (1995). Carretta *et al.* (2000b), Cacciari & Clementini (2003), and Di Criscienzo *et al.* (2006) discuss more recent results.

Four methods have generally been applied to the problem of Pop II distances: trigono-

metric parallaxes, cluster-based distances, statistical parallaxes, and surface brightness analyses. In the following we will use the absolute magnitude at $[\text{Fe}/\text{H}] = -1.5$ to inter-compare methods.

- **Trigonometric Parallaxes** are essentially free from complicating assumptions. However, one must still consider whether the instability region is sufficiently populated by the few data to give an unbiased relation. The first reliable parallax of an RRL came from the *HIPPARCOS* satellite. The Koen & Laney (1998) result is from an analysis of Hipparcos parallaxes of RRL. Fernley et al. (1998a) used the parallax for RR Lyr itself (with an adopted $[\text{Fe}/\text{H}] = -1.39$) of 4.38 ± 0.59 mas to estimate $M_V = 0.78 \pm 0.29$ mag. *HIPPARCOS* also determined a distance to our target CP2 with 10–13% errors. There are now two versions of the *Hipparcos* catalog: Perryman et al. (1997) (HIP97) and van Leeuwen (2007) (HIP07). We have reanalyzed the field for RR Lyr itself, which benefitted from additional FGS data secured in late 2008. The Benedict et al. (2002b) *HST* parallax provided $M_V = 0.61 \pm 0.11$, compared to our new value, $M_V = 0.54 \pm 0.07$. Because the new and old parallaxes agree within their respective errors (Section 4.3.2), we ascribe the difference in M_V primarily to a newer and presumably more accurate extinction determination, $A_V = 0.13$ (Kolenberg et al. 2010). HIP97 and HIP07 parallaxes can be compared with the present *HST* results in Tables 7 and 8.

Gratton (1998) derived an RRL scale based on the Hipparcos parallaxes of field horizontal branch stars. The value in Table 10 is a slight update of this result (Carretta et al. 2000).

- **Cluster-based distances** generally rely upon main sequence or horizontal branch fitting calibrated by stars with well-determined distances. Using *Hipparcos* parallaxes of 56 subdwarfs and data for 9 globular clusters, Carretta et al. (2000) obtain distances and hence the absolute magnitudes of the RRLs the clusters contain. Their result (Table 10) agrees well with ours, though their errors are large. Thus our results promise improved accuracy in cluster distances.
- **Statistical Parallaxes** are derived by combining proper motions and radial velocities. Fernley et al. (1998b) performed such an analysis based on the Hipparcos proper motions. In an elaborate reanalysis of those data, Gould & Popowski (1998) confirmed the Fernley et al. result with a slightly smaller uncertainty. We quote the Gould & Popowski value in Table 10. There is about a 2 sigma difference from our value. This difference is not in itself of very high significance. However the consequences of adopting RRL absolute magnitudes 0.3 mag brighter than that suggested by the statistical parallaxes is highly important for distance scale applications. The reason for the fainter result obtained from statistical parallaxes is not clear. However the

statistical work depends on the adoption of a Galactic model. The result may be due to deviations from the adopted model (due possibly to stellar streams in the Galactic Halo). A full analysis of the Galactic motions of RRLs based on our new absolute magnitude scale is desirable.

It is, however, interesting to note the work of Martin & Morrison (1998) who calculate the mean space motion (using radial velocities and proper motions) of Halo RRL with respect to the Sun as a function of the adopted absolute magnitude (their fig 6). The velocity (V) in the direction of galactic rotation is quite sensitive to the absolute magnitude. For our derived value of the absolute magnitude scale their results predicts $V = -250 \text{ km s}^{-1}$. The galactic rotational velocity (with respect to the Sun) was recently determined from VLBI of Galactic masers (Brunthaler et al. 2011) as $246 \pm 7 \text{ km s}^{-1}$. Our absolute magnitude scale implies that the halo RRL form a non-rotating system. Earlier values of the galactic rotation were smaller, and our result would have implied a retrograde halo.

Lastly, Dambis (2009) obtained a calibration of a K -log P relation from statistical parallaxes which yields an $M_K \sim 0.4 \text{ mag}$ fainter than our result. This suggests that the difference in M_V , comparing statistical parallaxes and our trigonometric work, is not due to problems with corrections for interstellar absorption.

- **Surface Brightness** Extending the early efforts of Baade and Wesselink, Barnes & Evans (1976) introduced a technique for determining pulsating star distances using differential surface brightness measurements. There are two main uncertainties in the application of this general method to RRL. First, shocks occurring in the atmospheres of the stars during part of the pulsation cycle complicate the interpretation of the radial velocity curves. Secondly, it is necessary to adopt a value of p (the ratio of pulsation velocity to measured radial velocity) and this remains uncertain. Also, not all color indices are equally effective in predicting a surface brightness. In addition to a result based on many RRL from Fernley et al. (1998b), the present status of the RRL M_V from this method is captured in the paper by Cacciari & Clementini (2003), who have introduced a number of refinements, but their work is for only one star, RR Cet. Our parallaxes may produce a more accurate p factor for RRL, and may refine p for CP2.

7. Distance Scale Applications

We now apply our new zero-points to several globular clusters and the LMC. The globular clusters were chosen because they had existing RRL photometry in both the V- and the K-band. We also estimate globular cluster ages with these new distance moduli. All

parameterizations, sources of slopes and zero-points, and distance moduli derived from our new RRL absolute magnitudes listed in Table 8 and plotted in Figures 6 and 7 are summarized in Table 11 (Globular Clusters) and Table 12 (LMC). In each case we assume that $A_V=3.1E(B-V)$, and $A_K=0.11A_V$.

7.1. Distance Moduli of Globular Clusters

A sample of six globular clusters was selected based on the availability of both K-band and V-band RRL photometry. We first employ the zero-point from M_K versus $\log P$, our Figure 6, comparing with the apparent magnitude PLR for each cluster. To each we also apply the $M_V - [Fe/H]$ relation shown in Figure 7, transforming the relevant $[Fe/H]$ from Sollima et al. (2006) on the CG scale to the ZW scale, using the CG-ZW mapping established by Carretta & Gratton (1997) (their equation 7). The final M_V error includes the ± 0.047 magnitude $M_V - [Fe/H]$ slope error. The error in our adopted K-band PLR slope makes a negligible contribution to the final distance modulus error. The expectation is that the K and V distance moduli collected in Table 11 should agree. In all cases the two approaches yield the same distance modulus within the errors.

M3 From Benkő et al. (2006) we extract for RRL $\langle V_0 \rangle = 15.62 \pm 0.05$, corrected for an assumed $A_V = 0.03$. The Figure 7 $M_V - [Fe/H]$ and an $[Fe/H] = -1.34$ (CG), $[Fe/H] = -1.57$ (ZW) provide $M_V = 0.45 \pm 0.05$, thus $(m-M)_0 = 15.17 \pm 0.12$. The Butler (2003) K-band apparent magnitude PLR zero-point is 13.93 ± 0.04 . This, combined with our Figure 6 zero-point yields $(m-M)_0 = 15.16 \pm 0.06$.

M4 For RRL Cacciari (1979) find $\langle V_0 \rangle = 12.15 \pm 0.06$, corrected for an assumed $A_V = 1.19$. The Figure 7 $M_V - [Fe/H]$ and an $[Fe/H] = -1.40$ (ZW) provide $M_V = 0.47 \pm 0.05$, thus $(m-M)_0 = 11.68 \pm 0.13$. The Longmore et al. (1990) K-band apparent magnitude at $\log P = -0.3$ (figure 1f) is $K(0) = 11.10 \pm 0.06$, corrected for $A_K = 0.13$. This, combined with our Figure 6 zero-point yields $(m-M)_0 = 11.48 \pm 0.08$. The two approaches barely yield the same distance modulus within the errors, possibly due to the high and uncertain extinction correction due to known differential reddening. We note that increasing to $E(B-V) = 0.415$ (from the adopted 0.36) equalizes the two distance moduli at $(m-M)_0 = 11.46$.

M15 From Silbermann & Smith (1995), table 6, we derive $\langle V_0 \rangle = 15.51 \pm 0.02$, corrected for an assumed $A_V = 0.30$. This value comes only from the RRL ab stars. The Figure 7 $M_V - [Fe/H]$ and an $[Fe/H] = -2.16$ (ZW) provide $M_V = 0.31 \pm 0.05$, thus $(m-M)_0 = 15.20 \pm 0.09$. The Longmore et al. (1990) K-band apparent magnitude at $\log P = -0.3$ (their figure 1c) is $K_0 = 14.67 \pm 0.10$, corrected for $A_K = 0.03$. This, combined with our Figure 6 zero-point yields

$$(m-M)_0=15.18\pm0.11.$$

M68 From Walker (1994) we obtain $\langle V_0 \rangle = 15.51 \pm 0.01$, corrected for an assumed $A_V = 0.13$. The Figure 7 $M_V - [\text{Fe}/\text{H}]$ and an $[\text{Fe}/\text{H}] = -2.08$ (ZW) provide $M_V = 0.33 \pm 0.05$, thus $(m-M)_0 = 15.18 \pm 0.08$. The Dall’Ora et al. (2006) K-band apparent magnitude at $\log P = -0.2$ (their figure 3) is $K_0 = 14.35 \pm 0.04$, corrected for $A_K = 0.01$. This, combined with our Figure 6 zero-point yields $(m-M)_0 = 15.10 \pm 0.06$.

ω **Cen** Del Principe et al. (2006) (figure 4) provides $\langle K_0 \rangle = 13.05 \pm 0.06$ for RRL ab at $\log P = -0.2$. At that $\log P$ the Figure 6 PLR yields $M_K(0) = -0.75 \pm 0.05$. Hence, $(m-M)_0 = 13.80 \pm 0.08$. Adopting $[\text{Fe}/\text{H}] = -1.84$ (ZW), we obtain $M_V(0) = +0.38$ from Figure 7. RRL V-band photometry from Olech et al. (2003) and $A_V = 0.36$ (Sollima et al. 2006) provide $\langle V_0 \rangle = 14.20 \pm 0.02$, and $(m-M)_0 = 13.82 \pm 0.09$.

M92 From Kopacki (2001) we derive $\langle V_0 \rangle = 15.01 \pm 0.08$, corrected for an assumed $A_V = 0.08$. The Figure 7 $M_V - [\text{Fe}/\text{H}]$ and an $[\text{Fe}/\text{H}] = -2.16$ (ZW) provide $M_V = 0.31 \pm 0.05$, thus $(m-M)_0 = 14.70 \pm 0.11$. The Del Principe et al. (2005) K-band apparent magnitude at $\log P = -0.19$ is $K_0 = 13.86 \pm 0.04$, corrected for $A_K = 0.01$. This, combined with our Figure 6 zero-point yields $(m-M)_0 = 14.64 \pm 0.06$. The two approaches yield the same distance modulus within the errors.

Within a year or so we will have an independent check on these globular cluster distance moduli. Chaboyer et al. (2011) are using the FGS on *HST* to obtain parallaxes of 9 metal-poor ($[\text{Fe}/\text{H}] < -1.5$) main sequence stars. The *HST* parallaxes are expected to have accuracies similar to those achieved for this RRL project, leading to absolute magnitude uncertainties of ± 0.05 mag for a given star. These stars will be used to test metal-poor stellar evolution models and to determine main sequence fitting distances to a large number of low metallicity globular clusters, including those above. See McArthur et al. (2011) for an example of the construction of a main sequence using only a few highly precise absolute magnitudes.

7.2. Globular Cluster Ages

Adopting the K-band distance moduli from Table 11, we calculate absolute ages for our selected globular clusters using a Monte Carlo simulation similar to that described by Chaboyer et al. (1998). We did not estimate an age for ω Cen, as the cluster is very complex with multiple stellar populations, and not conducive to a simple age determination. For each remaining globular cluster, 3000 sets of isochrones were generated using the Dartmouth stellar evolution program (Chaboyer et al. 2001; Bjork & Chaboyer 2006; Dotter et al. 2008). The input parameters for each set of isochrones were randomly selected from their distribu-

tion function as discussed by Bjork & Chaboyer (2006). A total of 21 different parameters were varied in the stellar evolution calculations, including the nuclear reaction rates, opacities, surface boundary conditions, mixing length and composition. The $[\text{Fe}/\text{H}]$ values used in the stellar models were selected from a Gaussian distribution with a standard deviation of 0.15 dex and a mean based upon high resolution spectroscopic abundance analysis of FeI lines (Carretta et al. 2009) and FeII lines (Kraft & Ivans 2003). These independent $[\text{Fe}/\text{H}]$ measurements agree quite well with each other for each of the globular clusters, and the mean of the two measurements were used in the stellar model calculations⁵.

The age of each globular cluster was determined using the absolute magnitude of the point on the subgiant branch which is 0.05 mag redder than the turn-off (Chaboyer et al. 1996). Photometry in V and I for each globular cluster except M15 was obtained from P.B. Stetson’s photometric standard fields⁶ and used to determine the apparent magnitude of the subgiant branch. The Stetson database for M15 does not reach the main sequence turn-off in I. For this cluster, we used the HST ACS photometry from Anderson et al. (2008). The V band distance modulus for each cluster was determined using the true distance moduli (derived from the K band) and reddening listed in Table 11. Errors in the distance moduli were assumed to be Gaussian with the uncertainty given in Table 11, with the exception of M4. M4 has a fairly high reddening, and there is evidence for differential reddening across the clusters. Estimates for absorption in the V band range from $A_V = 1.16$ mag (using $E(B-V) = 0.36$ and the extinction calculator from McCall 2004) to $A_V = 1.33$ mag (Richer et al. 1997). We elected to use $A_V = 1.22 \pm 0.08$ mag, which implies an uncorrected $(m - M)_V = 12.70 \pm 0.11$ mag for M4. Lastly, the age error for M15 was derived from the smaller error on the V-band distance modulus.

We determined the ages (collected in Table 11) of the clusters to be: M3 10.8 ± 1.0 Gyr; M4 ($11.1_{-1.4}^{+1.7}$) Gyr; M15 12.1 ± 1.0 Gyr; M68 12.4 ± 1.0 Gyr; and M92 13.1 ± 1.1 Gyr. The larger error in the age of M4 is due to the larger uncertainty in the V band distance modulus to this cluster.

Our absolute ages are in reasonable agreement with previous estimates. For example, di Cecco et al. (2010) found an absolute age of 11.0 ± 1.5 Gyr for M92, which agrees

⁵The high resolution spectroscopic $[\text{Fe}/\text{H}]$ determinations for each cluster differ somewhat from the ZW scale listed in Table 11. Those $[\text{Fe}/\text{H}]$ values were selected to be on the same $[\text{Fe}/\text{H}]$ system as the target parallax stars (which, in general, do not have high dispersion spectroscopic $[\text{Fe}/\text{H}]$ determinations). For the purposes of stellar model calculations, the consistency between the field stars and globular clusters stars is not an issue, rather one is interested in the absolute $[\text{Fe}/\text{H}]$ scale, which is best determined from high resolution spectroscopic studies.

⁶<http://www4.cadc-ccda.hia-ihp.nrc-cnrc.gc.ca/community/STETSON/standards/>

within the uncertainties with our age. The differences between our age estimate and that of di Cecco et al. (2010) is due our use of an updated nuclear reaction rate, and a different distance modulus. di Cecco et al. (2010) used the older NACRE rate for the $^{14}\text{N}(p, \gamma)^{15}\text{O}$ nuclear reaction. We used the updated value for this critical nuclear reaction rate from Marta et al. (2008), which yields globular cluster ages approximately 1 Gyr older than the reaction rate used by di Cecco et al. di Cecco et al. (2010) adopted a distance modulus of 14.74 (no error reported), which is 0.1 mag larger than the distance modulus derived in this work. An increase in the distance modulus by 0.1 mag will decreased derived ages by approximately 1 Gyr. The distance modulus adopted by di Cecco et al. (2010) was the one that gave the best fit between their theoretical isochrones and the observed color-magnitude diagrams. It depends critically on their transformations for theoretical luminosities and temperatures to observed magnitudes and colors.

In general, it is difficult to find absolute age determinations for globular clusters in the literature. Most works focus on relative age determinations, and the errors in the age estimates do not include uncertainties in the stellar evolution models and isochrones. Although they focused on relative age determinations, Salaris & Weiss (2002) carefully determined the ages of a large sample of globular clusters, including all of the clusters whose ages are determined in this paper. The difference between our ages and those derived by Salaris & Weiss (2002) are within the errors: M92 0.3 ± 1.4 Gyr; M68 1.2 ± 1.3 Gyr; M3 -0.5 ± 1.2 Gyr; M15: 0.3 ± 1.4 Gyr and M4 0.1 ± 1.7 Gyr.

M3 is the only cluster we find to have a younger age than that derived by Salaris & Weiss (2002). This is likely due to the fact that the distance modulus we derive for this cluster is of order 0.1 mag larger than previous estimates, leading to our determination of a relatively young age for this cluster. Such a young age is supported by the fact that M3 has a relatively red horizontal branch morphology for its metallicity. A detailed differential study of M3 and M13 (clusters with similar metallicities) by Rey et al. (2001) found that M3 was 1.7 ± 0.7 Gyr younger than M13. The biggest age difference between our work and Salaris & Weiss (2002) is for the globular cluster M68. Salaris & Weiss (2002) used $[\text{Fe}/\text{H}] = -2.00$ for this cluster while we adopt $[\text{Fe}/\text{H}] = -2.33 \pm 0.15$ dex based upon more recent spectroscopic studies. Using $[\text{Fe}/\text{H}] = -2.00$ in our stellar evolution models reduces our age estimate for M68 by 1.1 Gyr to 11.3 Gyr and leads to good agreement with the Salaris & Weiss (2002) age estimate of this cluster of 11.2 Gyr.

7.3. LMC Distance Moduli

In this section we derive the distance modulus of the LMC using our derived RRL absolute magnitudes. We then compare it with that derived from classical Cepheids whose absolute magnitudes were also based on *HST* trigonometrical parallaxes (Benedict et al. 2007).

From observations of RRL in the LMC Gratton et al. (2004) derived the relation

$$V_0 = (0.214 \pm 0.047)([Fe/H] + 1.5) + 19.064 \pm 0.017 \quad (15)$$

with metallicities on the ZW scale. This with the results in line 7 of Table 9 yields a true distance modulus of 18.61 ± 0.05 (Table 12) from the LKH approach. The OGLE team (Soszynski et al. 2003) found a mean value of $V_0 = 18.90 \pm 0.02$ for 7110 RRab and c stars in the LMC. This is from the OGLEII survey. The mean RRL magnitude (uncorrected for reddening) is not changed in the larger OGLEIII survey (Soszyński et al. 2009). Using the Gratton relation and adopting a mean metallicity of -1.53 for the LMC from Borissova et al. (2009) together with the zero points of Table 9 leads to an LMC modulus of 18.46 ± 0.06 . The differences between these two results for the LMC modulus is primarily due to the fact that the two groups adopt different reddenings for the LMC objects (see Clementini et al. 2003).

For the infrared we have used the Borissova et al. (2009) work which has individual values of $[Fe/H]$ and incorporates earlier work. Using Equation 13 with a zero point corresponding to $a_6 = -0.54$ they obtain an LMC modulus of 18.53. The LK corrected zero-point in Table 9 then shows that our modulus is 0.02 mag brighter. We adopt 18.55 ± 0.05 based on the uncertainty of our zero-point and the uncertainty in the infrared data. The result using the reduced parallax zero-point is 18.53. The reddenings adopted by Borissova et al. were means of values derived in a variety of ways. The uncertainties in these values have a very small effect (of order 0.01 mag) on the derived distance modulus.

In view of the sensitivity of the derived LMC modulus to the reddening when using the relation in V, it seems best to give most weight to the determination using the relation in K. While we believe that this is the current best mean distance to the LMC from RR Lyraes, it should be noted that the LMC is sufficiently close that its depth structure is important. Thus strictly, the result applies to the selection of stars studied by Borissova et al. and the model of the LMC that they adopt. A similar remark applies to other determinations.

Dall’Ora et al. (2004) established a K-Band PLR in the Reticulum cluster associated with the LMC.

$$K_0 = -2.16 \log P + 17.33 \pm 0.03 \quad (16)$$

This, together with a_4 in Table 9, leads to a corrected distance modulus for the cluster of 18.50 ± 0.03 . As discussed by Dall’Ora et al. the relative distance of this cluster and the main body of the LMC has not been well established. Our result suggests that any difference in distance is small.

In view of the above discussion we adopt 18.55 ± 0.05 (LKH method) or 18.53 (reduced parallax method) as the best RRL distance to the LMC. This may be compared with the LMC modulus obtained by Benedict et al. (2007) from classical Cepheids based on *HST* parallaxes of Galactic stars of this type. Their results were $(m-M)_0 = 18.50 \pm 0.04$ from a PL relation in W_{VI} ; 18.52 ± 0.06 from a PL relation in V_0 ; and 18.48 ± 0.04 from a PL relation in K_0 . These results have not been corrected for the metallicity difference between the LMC Cepheids and the Galactic calibrating stars. There has been much discussion as to whether or not a metallicity correction to Cepheid absolute magnitudes is necessary. The above results show that any correction is small; at least between Cepheids of Galactic and LMC metallicities. This result agrees with the theoretical discussion of Bono et al. (2010).

We note that recent work (Laney & Pietrzyński 2009) on the absolute magnitude calibration of red clump stars, which formerly led to a rather low modulus for the LMC, now gives $(m-M)_0 = 18.47 \pm 0.03$ in good agreement with the RRL and (uncorrected for metallicity) Cepheid results.

8. The Type 2 Cepheids

In this section we discuss the two CP2 for which we have obtained parallaxes and absolute magnitudes. Matsunaga et al. (2006) established an M_K - $\log P$ relation for CP2s in globular clusters which shows little evidence of a metallicity dependence. It was therefore originally anticipated that the parallaxes of these two stars, κ Pav ($\log P = 0.958$) and VY Pyx ($\log P = 0.093$) could be used to establish a zero-point for this relation, which appears to be continuous with a PL relation for RRLs. Subsequent work (Soszyński et al. 2009; Matsunaga et al. 2009) has shown that in the LMC field the situation is more complex than in globular clusters. Some CP2 with periods near that of κ Pav lie above the PL relation, and have distinctive light curves (peculiar W Vir stars). Many of these stars are known to be binaries. It has now been suggested (Feast et al. 2008) that κ Pav belongs to this class, though it is not known to be binary and the classification remains uncertain.

The identification of a star as belonging to an older stellar population can be based on kinematics and/or metallicity. The RRL transverse velocities, V_t in Table 8, all suggest an identification with the halo, or that these stars have no connection with the local stellar thin

disk population. As summarized in Maas et al. (2007), the identification of CP2 is more complex. First, there is separation by period and metallicity. The prototype short-period CP2 is BL Her with $P=1.31^d$ and $[\text{Fe}/\text{H}]=-0.1$ (Maas et al. 2007). The long-period prototype CP2 is W Vir with $P=17.27^d$ and $[\text{Fe}/\text{H}]=-1.0$ (Barker et al. 1971). In addition to detailed metallicity variations by species the classification of CP2 also rests on distance from the Galactic plane, $|Z|$. The Galactic latitudes of VY Pyx and κ Pav, $+13.6$ and -25.4 respectively, together with the Table 7 parallaxes, yield Z values of 36.5pc and 77pc, not particularly extreme. Nor are the transverse velocities of VY Pyx and κ Pav (Table 7) indicative of halo or thick disk membership. The metallicity of κ Pav, $[\text{Fe}/\text{H}]=0.0$ (Luck & Bond 1989) is far from the prototypical $[\text{Fe}/\text{H}]=-1$. In contrast our newly measured metallicity for VY Pyx ($[\text{Fe}/\text{H}]=-0.01$, Table 1) is the same as that measured by Maas et al. (2007) for the prototype BL Her (though their value for VY Pyx is -0.4).

Figure 6 shows an M_K - $\log P$ relation. The slope (-2.38 ± 0.04) was derived by Sollima et al. (2006) from RRLs in globular clusters. This is essentially the same as the slope found by Matsunaga et al. (2006) for CP2s in globular clusters (-2.41 ± 0.05). The zero-point was fixed by our RRLs which are shown. This relation passes within 0.01mag of our absolute magnitude of κ Pav, which is also plotted, although this star was not used in deriving the zero-point. This suggests that either κ Pav is not a peculiar W Vir star, or is one of the few that lie near the PL relation. It is very desirable to clear up this matter. If it can be used as a normal CP2, it would add significantly to the distance scale calibration.

VY Pyx at M_K , $\log P = -0.26$, 0.0934 lies $+1.19 \pm 0.08$ mags below the regression line of Figure 6. A weighted average of HIP 97 and HIP07 parallaxes ($\pi_{abs} = 5.37 \pm 0.38$) gives $M_K = -0.68 \pm 0.16$ which is $+0.78$ magnitudes below the regression line. It is not clear whether this star indicates that a wide range of absolute magnitudes is possible for short period CP2s, or whether it is a rare anomaly. Detailed studies of CP2s with periods near one day in the Magellanic Clouds may answer this question.

9. Summary

1. *HST* astrometry has now yielded absolute trigonometric parallaxes for 5 RRL variables and two CP2 with an average $\sigma_\pi = 0.18$ mas, or $\sigma_\pi/\pi = 5.4\%$. These parallaxes, along with precision photometry culled from the literature, Lutz-Kelker-Hanson bias corrections, and reddening corrections derived from both the literature and/or our ancillary spectrophotometry, provide absolute magnitudes with which to extract zero-points for a Period-Luminosity Relation and an M_V - $[\text{Fe}/\text{H}]$ relation. The restricted ranges of both $\log P$ and $[\text{Fe}/\text{H}]$ preclude solving for slopes. Adopting previously determined

slopes, our zero-point errors are now at or below 0.03 magnitudes in the K bandpass and 0.05 in the V bandpass.

2. To obtain these parallaxes, no RRL or CP2 required the addition of a perturbation orbit in the modeling.
3. The CP2 κ Pav ($\log P = 0.96$) lies within 0.01 magnitude of the value predicted by an extrapolation of an RRL $K_s - \log P$ relation based on a slope derived from globular clusters and our parallax zero-point. This star could be an important distance scale calibrator, if the uncertainty regarding its nature (normal or peculiar CP2) can be resolved. This situation appears to support the assertion that RRL and CP2 together can establish a single PLR (Matsunaga et al. 2006; Majaess 2010).
4. Our absolute magnitude of the CP2 star VY Pyx ($\log P = 0.093$) falls well below a $K_s - \log P$ relation for RRLs based on our zero-point. This result is not currently understood but we see no reason to question the accuracy of our parallax.
5. We apply our V and K calibrations to selected galactic globular clusters. We obtain K-band PLR and $M_V - [\text{Fe}/\text{H}]$ distance moduli that agree within the errors for all clusters. Ages obtained from stellar evolution models range 10.8 – 13.1 Gy.
6. Based on the $K_s - [\text{Fe}/\text{H}] - \log P$ relation of Borissova et al. (2009) and with our zero-point calibration, we derive an LMC distance modulus of $(m-M)_0 = 18.55 \pm 0.05$. This result agrees within the errors with that derived from classical Cepheids, calibrated by *HST* parallaxes (Benedict et al. 2007) and uncorrected for metallicity differences between the Galactic calibrators and the LMC Cepheids.

Support for this work was provided by NASA through grants GO-11211 and GO-11789 from the Space Telescope Science Institute, which is operated by AURA, Inc., under NASA contract NAS5-26555. This paper uses observations made at the South African Astronomical Observatory (SAAO), and observations obtained with the Apache Point Observatory 3.5-meter telescope, which is owned and operated by the Astrophysical Research Consortium. This paper uses observations made at the Cerro Tololo Observatory 4m telescope. Cerro Tololo is also operated by AURA. TEH thanks the SMARTS crew for obtaining photometry of the VY Pyx and UV Oct fields after three weathered-out failed attempts by TEH. This publication makes use of data products from the Two Micron All Sky Survey, which is a joint project of the University of Massachusetts and the Infrared Processing and Analysis Center/California Institute of Technology, funded by NASA and the NSF. This research has made use of the SIMBAD database, operated at CDS, Strasbourg, France; the NASA/IPAC

Extragalactic Database (NED) which is operated by JPL, California Institute of Technology, under contract with the NASA; and NASA’s Astrophysics Data System Abstract Service. This material is based in part upon work by TGB while serving at the National Science Foundation. Any opinions, findings, and conclusions or recommendations expressed in this material are those of the authors and do not necessarily reflect the views of the National Science Foundation. This work is supported by an STFC Rolling Grant (L.F.). O.K. is a Royal Swedish Academy of Sciences Research Fellow supported by grants from the Knut and Alice Wallenberg Foundation and the Swedish Research Council. D.S. acknowledges support received from the Deutsche Forschungsgemeinschaft (DFG) Research Grant RE1664/7-1. KK, LF and NN are supported by Austrian FWF grants T359 and P19962. Feast and Menzies thank the National Research Foundation (NRF) of South Africa for financial support. GFB thanks Debbie Winegarten, whose able assistance with other matters freed me to devote necessary time to this project. Finally we thank an anonymous referee for careful reading and extensive constructive criticism which materially improved the presentation and discussion.

REFERENCES

- Alcock C., Alves D.R., Becker A., et al., 2003. ApJ, 598, 597
- Anderson J., Sarajedini A., Bedin L.R., et al., 2008. AJ, 135, 2055
- Barcza S., 2002. A&A, 384, 460
- Barker T., Baumgart L.D., Butler D., et al., 1971. ApJ, 165, 67
- Barnes T.G., 2009. In J.A. Guzik & P.A. Bradley, eds., *Stellar Pulsation: Challenges for Theory and Observation*, vol. 1170, 3–12. AIP
URL <http://link.aip.org/link/?APC/1170/3/1>
- Barnes T.G. & Evans D.S., 1976. MNRAS, 174, 489
- Benedict G.F., McArthur B., Nelan E., et al., 1998. AJ, 116, 429
- Benedict G.F., McArthur B.E., Bean J.L., et al., 2010. AJ, 139, 1844
- Benedict G.F., McArthur B.E., Feast M.W., et al., 2007. AJ, 133, 1810
- Benedict G.F., McArthur B.E., Fredrick L.W., et al., 2002a. AJ, 124, 1695
- Benedict G.F., McArthur B.E., Fredrick L.W., et al., 2002b. AJ, 123, 473
- Benkő J.M., Bakos G.Á., & Nuspl J., 2006. MNRAS, 372, 1657
- Bessell M.S. & Brett J.M., 1988. PASP, 100, 1134
- Bjork S.R. & Chaboyer B., 2006. ApJ, 641, 1102
- Bono G., Caputo F., Castellani V., et al., 2003. MNRAS, 344, 1097
- Bono G., Caputo F., & Di Criscienzo M., 2007. A&A, 476, 779
- Bono G., Caputo F., Marconi M., et al., 2010. ApJ, 715, 277
- Borissova J., Rejkuba M., Minniti D., et al., 2009. A&A, 502, 505
- Brunthaler A., Reid M.J., Menten K.M., et al., 2011. Astronomische Nachrichten, 332, 461
- Butler D.J., 2003. A&A, 405, 981
- Cacciari C., 1979. AJ, 84, 1542

- Cacciari C. & Clementini G., 2003. In D. Alloin & W. Gieren, ed., *Stellar Candles for the Extragalactic Distance Scale*, vol. 635 of *Lecture Notes in Physics*, Berlin Springer Verlag, 105–122
- Cacciari C., Corwin T.M., & Carney B.W., 2005. *AJ*, 129, 267
- Carretta E., Bragaglia A., Gratton R., et al., 2009. *A&A*, 508, 695
- Carretta E. & Gratton R.G., 1997. *A&AS*, 121, 95
- Carretta E., Gratton R.G., & Clementini G., 2000. *MNRAS*, 316, 721
- Chaboyer B., Demarque P., Kernan P.J., et al., 1996. *MNRAS*, 283, 683
- Chaboyer B., Demarque P., Kernan P.J., et al., 1998. *ApJ*, 494, 96
- Chaboyer B., Fenton W.H., Nelan J.E., et al., 2001. *ApJ*, 562, 521
- Chaboyer B.C., Benedict G.F., McArthur B.E., et al., 2011. In *American Astronomical Society Meeting Abstracts #217*, vol. 43 of *Bulletin of the American Astronomical Society*, 242.25
- Clementini G., Gratton R., Bragaglia A., et al., 2003. *AJ*, 125, 1309
- Cox A.N., 2000. *Allen’s Astrophysical Quantities*. AIP Press
- Dall’Ora M., Bono G., Storm J., et al., 2006. *Mem. Soc. Astron. Italiana*, 77, 214
- Dall’Ora M., Storm J., Bono G., et al., 2004. *ApJ*, 610, 269
- Dambis A.K., 2009. *MNRAS*, 396, 553
- Del Principe M., Piersimoni A.M., Bono G., et al., 2005. *AJ*, 129, 2714
- Del Principe M., Piersimoni A.M., Storm J., et al., 2006. *ApJ*, 652, 362
- di Cecco A., Becucci R., Bono G., et al., 2010. *PASP*, 122, 991
- Di Criscienzo M., Caputo F., Marconi M., et al., 2006. *MNRAS*, 365, 1357
- Dotter A., Chaboyer B., Jevremović D., et al., 2008. *ApJS*, 178, 89
- Epps E.A. & Sinclair J.E., 1973. *The Observatory*, 93, 78
- Feast M., 2002. *MNRAS*, 337, 1035

- Feast M.W., 2010. In C. Sterken, N. Samus, & L. Szabados, ed., *Variable Stars, the Galactic halo and Galaxy Formation*, 45
- Feast M.W., Laney C.D., Kinman T.D., et al., 2008. MNRAS, 386, 2115
- Fernley J., Barnes T.G., Skillen I., et al., 1998a. A&A, 330, 515
- Fernley J., Skillen I., Carney B.W., et al., 1998b. MNRAS, 293, L61
- Gould A. & Morgan C.W., 2003. ApJ, 585, 1056
- Gould A. & Popowski P., 1998. ApJ, 508, 844
- Gratton R.G., 1998. MNRAS, 296, 739
- Gratton R.G., Bragaglia A., Clementini G., et al., 2004. A&A, 421, 937
- Hanson R.B., 1979. MNRAS, 186, 875
- Hardie R.H., 1955. ApJ, 122, 256
- Holtzman J.A., Harrison T.E., & Coughlin J.L., 2010. *Advances in Astronomy*, 2010
- Jefferys W.H., Fitzpatrick M.J., & McArthur B.E., 1988. *Celestial Mechanics*, 41, 39
- Koen C. & Laney D., 1998. MNRAS, 301, 582
- Kolenberg K., Fossati L., Shulyak D., et al., 2010. A&A, 519, 64
- Kolenberg K., Smith H.A., Gazeas K.D., et al., 2006. A&A, 459, 577
- Kopacki G., 2001. A&A, 369, 862
- Kraft R.P. & Ivans I.I., 2003. PASP, 115, 143
- LaCluyzé A., Smith H.A., Gill E., et al., 2004. AJ, 127, 1653
- Laney C.D. & Pietrzyński G., 2009. In J. A. Guzik & P. A. Bradley, ed., *American Institute of Physics Conference Series*, vol. 1170 of *American Institute of Physics Conference Series*, 34–36
- Layden A.C., 1994. AJ, 108, 1016
- Lindegren L., Babusiaux C., Bailer-Jones C., et al., 2008. In W. J. Jin, I. Platais, & M. A. C. Perryman, ed., *IAU Symposium*, vol. 248 of *IAU Symposium*, 217–223

- Longmore A.J., Dixon R., Skillen I., et al., 1990. MNRAS, 247, 684
- Longmore A.J., Fernley J.A., & Jameson R.F., 1986. MNRAS, 220, 279
- Luck R.E. & Bond H.E., 1989. ApJ, 342, 476
- Lutz T.E. & Kelker D.H., 1973. PASP, 85, 573
- Maas T., Giridhar S., & Lambert D.L., 2007. ApJ, 666, 378
- Majaess D.J., 2010. Journal of the American Association of Variable Star Observers (JAAVSO), 38, 100
- Marta M., Formicola A., Gyürky G., et al., 2008. Phys. Rev. C, 78, 022802
- Martin J.C. & Morrison H.L., 1998. AJ, 116, 1724
- Matsunaga N., Feast M.W., & Menzies J.W., 2009. MNRAS, 397, 933
- Matsunaga N., Fukushi H., Nakada Y., et al., 2006. MNRAS, 370, 1979
- McArthur B., Benedict G.F., Jefferys W.H., et al., 2002. In S. Arribas, A. Koekemoer, & B. Whitmore, eds., *The 2002 HST Calibration Workshop : Hubble after the Installation of the ACS and the NICMOS Cooling System*, 373
- McArthur B.E., Benedict G.F., Harrison T.E., et al., 2011. AJ, 141, 172
- McArthur B.E., Benedict G.F., Lee J., et al., 2001. ApJ, 560, 907
- McCall M.L., 2004. AJ, 128, 2144
- Nelan E.P., 2010. *Fine Guidance Sensor instrument Handbook*. STScI, Baltimore, MD, 17 ed.
- Oaster L., Smith H.A., & Kinemuchi K., 2006. PASP, 118, 405
- Olech A., Kaluzny J., Thompson I.B., et al., 2003. MNRAS, 345, 86
- Perryman M.A.C., Lindegren L., Kovalevsky J., et al., 1997. A&A, 323, L49
- Rey S.C., Yoon S.J., Lee Y.W., et al., 2001. AJ, 122, 3219
- Richer H.B., Fahlman G.G., Ibata R.A., et al., 1997. ApJ, 484, 741
- Roeser S., Demleitner M., & Schilbach E., 2010. AJ, 139, 2440

- Salaris M. & Weiss A., 2002. *A&A*, 388, 492
- Sandage A., 1990. *ApJ*, 350, 603
- Sanwal N.B. & Sarma M.B.K., 1991. *Journal of Astrophysics and Astronomy*, 12, 119
- Savage B.D. & Mathis J.S., 1979. *ARA&A*, 17, 73
- Schlegel D.J., Finkbeiner D.P., & Davis M., 1998. *ApJ*, 500, 525
- Shobbrook R.R., 1992. *MNRAS*, 255, 486
- Silbermann N.A. & Smith H.A., 1995. *AJ*, 110, 704
- Smith H., 2003. *MNRAS*, 338, 891
- Smith H.A., 1995. *RR Lyrae stars*. Cambridge University Press
- Sollima A., Cacciari C., Arkharov A.A.H., et al., 2008. *MNRAS*, 384, 1583
- Sollima A., Cacciari C., & Valenti E., 2006. *MNRAS*, 372, 1675
- Soszynski I., Udalski A., Szymanski M., et al., 2003. *Acta Astron.*, 53, 93
- Soszyński I., Udalski A., Szymański M.K., et al., 2009. *Acta Astron.*, 59, 1
- Standish Jr. E.M., 1990. *A&A*, 233, 252
- Sturch C., 1966. *ApJ*, 143, 774
- Subasavage J.P., Bailyn C.D., Smith R.C., et al., 2010. In *Society of Photo-Optical Instrumentation Engineers (SPIE) Conference Series*, vol. 7737 of *Presented at the Society of Photo-Optical Instrumentation Engineers (SPIE) Conference*
- van Altena W.F., Lee J.T., & Hoffleit E.D., 1995. *The General Catalogue of Trigonometric [Stellar] Parallaxes*. New Haven, CT: Yale University Observatory 4th ed. (YPC95)
- van Leeuwen F., 2007. *Hipparcos, the New Reduction of the Raw Data*, vol. 350 of *Astrophysics and Space Science Library*. Springer
- Walker A.R., 1994. *AJ*, 108, 555
- Yong D. & Lambert D.L., 2003. *PASP*, 115, 796
- Zakrzewski B., Ogloza W., & Moskalik P., 2000. *Acta Astron.*, 50, 387

Zinn R. & West M.J., 1984. ApJS, 55, 45

Table 1. Target Properties

ID	log P	T ₀	⟨V⟩	⟨K _S ⟩ ^a	[Fe/H] ^b	A _V	A _K
RZ Cep (c) ^c	-0.51052	54793.0050	9.47	8.11	-1.77±0.2	0.78	
XZ Cyg (ab) ^d	-0.33107	54395.1020	9.68	8.72	-1.44 0.2	0.30	0.04
SU Dra (ab) ^e	-0.18018	54733.1510	9.78	8.62	-1.80 0.2	0.03	0.00
RR Lyr (ab) ^f	-0.24655	50749.2380	7.76	6.49	-1.41 0.13	0.13	0.01
UV Oct (ab) ^g	-0.26552	53570.4141	9.50	8.30	-1.47 0.11	0.28	0.03
VY Pyx (BLHer) ^h	0.09340	54406.4072	7.30	5.72	-0.01 0.15	0.15	0.02
κ Pav (WVir) ⁱ	0.95815	54705.9320	4.35	2.78	0.0 0.13	0.05	0.0

^aK_S from Feast et al. (2008), except where noted.

^b[Fe/H] on Zinn & West (1984) scale.

^cRZ Cep: T₀, Smith for this paper; [Fe/H], A_V, Fernley et al. (1998b)

^dXZ Cyg: Fernley et al. (1998b), Feast et al. (2008); logP, T₀ from LaCluyzé et al. (2004)

^eSU Dra: Fernley et al. (1998b), Feast et al. (2008)

^fRR Lyr: Fernley et al. (1998b), Feast et al. (2008); [Fe/H], A_V, Kolenberg et al. (2010)

^gUV Oct: Fernley et al. (1998b), Feast et al. (2008); logP, T₀ from FGS photometry; [Fe/H] derived as for RR Lyr for this paper

^hVY Pyx: Feast et al. (2008); ⟨K_S⟩ from Laney for this paper; T₀ from FGS photometry; [Fe/H] derived as for RR Lyr for this paper

ⁱκ Pav: Feast et al. (2008); T₀ from FGS photometry; [Fe/H], Luck & Bond (1989)

Table 2. Log of Observations, Apparent Magnitude, Estimated B-V, and Pulsational Phase

Set	mJD	V	B-V ^a	Phase	Set	mJD	V	B-V ^a	Phase
RZ Cep					XZ Cyg				
1	54287.60885	9.759	0.53	0.6121	1	54292.22174	10.092	0.40	0.5050
1	54287.62167	9.719	0.52	0.6536	1	54292.2351	10.129	0.40	0.5106
1	54287.63148	9.704	0.52	0.6854	1	54292.24162	10.115	0.41	0.5337
1	54287.6403	9.683	0.51	0.7140	1	54292.24659	10.126	0.41	0.5476
1	54287.65023	9.643	0.50	0.7462	2	54322.03022	9.976	0.38	0.3911
1	54287.65756	9.599	0.49	0.7699	2	54322.03628	9.996	0.39	0.4041
2	54342.38356	9.270	0.41	0.0718	2	54322.04291	10.020	0.39	0.4183
2	54342.39431	9.309	0.41	0.1066	2	54322.04787	10.036	0.39	0.4290
2	54342.40291	9.337	0.42	0.1345	2	54322.05285	10.051	0.39	0.4396
2	54342.41148	9.363	0.42	0.1623	2	54322.05709	10.064	0.39	0.4487
2	54342.41535	9.375	0.42	0.1748	3	54348.96281	9.430	0.24	0.1136
2	54342.4233	9.402	0.43	0.2005	3	54348.96887	9.463	0.25	0.1266
2	54342.43593	9.440	0.44	0.2414	3	54348.97549	9.499	0.26	0.1408
3	54394.32964	9.596	0.48	0.3673	3	54348.98044	9.525	0.27	0.1514
3	54394.34037	9.635	0.49	0.4020	3	54348.98544	9.553	0.28	0.1621
3	54394.34896	9.667	0.50	0.4299	3	54348.98968	9.575	0.29	0.1712
3	54394.35756	9.696	0.50	0.4577	4	54395.08432	9.603	0.19	0.9621
3	54394.36141	9.706	0.51	0.4702	4	54395.09038	9.344	0.18	0.9751
3	54394.36936	9.721	0.51	0.4960	4	54395.097	9.105	0.17	0.9893
3	54394.382	9.732	0.52	0.5369	4	54395.10194	9.014	0.16	0.9999
4	54448.08932	9.731	0.52	0.5384	4	54395.10694	8.975	0.16	0.0106
4	54448.09977	9.725	0.53	0.5723	4	54395.11119	8.974	0.16	0.0197
4	54448.1081	9.716	0.53	0.5993	5	54489.86693	9.334	0.22	0.1020
4	54448.11644	9.705	0.53	0.6263	5	54489.87301	9.373	0.23	0.1151
5	54484.14804	9.588	0.47	0.3619	5	54489.87963	9.416	0.25	0.1292
5	54484.1585	9.628	0.49	0.3958	5	54489.88462	9.448	0.26	0.1399
5	54484.16683	9.659	0.49	0.4228	5	54489.88956	9.480	0.26	0.1505
5	54484.17516	9.686	0.50	0.4498	5	54489.89382	9.506	0.27	0.1597
6	54580.05927	9.309	0.41	0.0961	6	54516.76767	10.190	0.39	0.7562
6	54580.06972	9.350	0.42	0.1300	6	54516.77373	10.191	0.39	0.7692

Table 2—Continued

Set	mJD	V	B-V ^a	Phase	Set	mJD	V	B-V ^a	Phase
6	54580.07806	9.381	0.42	0.1570	6	54516.78035	10.189	0.38	0.7834
6	54580.08639	9.408	0.42	0.1840	6	54516.78532	10.190	0.37	0.7941
7	54622.23102	9.602	0.51	0.7246	6	54516.79029	10.193	0.36	0.8047
7	54622.24147	9.508	0.50	0.7585	6	54516.79454	10.196	0.36	0.8138
7	54622.2498	9.399	0.49	0.7855	7	54578.98769	9.417	0.22	0.1074
7	54622.25814	9.285	0.47	0.8125	7	54578.99372	9.444	0.23	0.1203
8	54677.10959	9.724	0.52	0.5208	7	54579.00032	9.476	0.25	0.1344
8	54677.12003	9.721	0.52	0.5546	7	54579.00529	9.500	0.26	0.1451
8	54677.12838	9.715	0.53	0.5817	7	54579.01028	9.524	0.27	0.1558
8	54677.1367	9.704	0.53	0.6086	7	54579.01453	9.543	0.27	0.1649
9	54730.0075	9.225	0.43	0.9000	8	54623.24464	9.588	0.21	0.9597
9	54730.01795	9.206	0.42	0.9339	8	54623.25071	9.472	0.19	0.9727
9	54730.02628	9.204	0.41	0.9609	8	54623.25734	9.341	0.18	0.9869
9	54730.03462	9.217	0.40	0.9879	8	54623.26228	9.254	0.17	0.9975
10	54778.54648	9.388	0.42	0.1571	8	54623.26728	9.196	0.17	0.0082
10	54778.55722	9.421	0.43	0.1919	8	54623.27152	9.167	0.16	0.0173
10	54778.56581	9.447	0.43	0.2198	9	54702.39156	10.112	0.41	0.5889
10	54778.5744	9.478	0.44	0.2476	9	54702.3966	10.118	0.41	0.5997
10	54778.57826	9.490	0.44	0.2601	9	54702.40324	10.130	0.42	0.6140
10	54778.58622	9.516	0.45	0.2859	9	54702.40819	10.138	0.42	0.6246
10	54778.59884	9.561	0.46	0.3268	9	54702.41318	10.145	0.42	0.6353
11	54837.09566	9.214	0.46	0.8454	9	54702.41742	10.151	0.42	0.6444
11	54837.10639	9.212	0.44	0.8802	10	54781.03128	9.368	0.23	0.1311
11	54837.11498	9.219	0.43	0.9080	10	54781.03465	9.390	0.24	0.1383
11	54837.12355	9.202	0.42	0.9358	10	54781.03947	9.422	0.25	0.1486
11	54837.12742	9.195	0.41	0.9483	10	54781.04615	9.466	0.26	0.1630
11	54837.13537	9.194	0.41	0.9741	10	54781.05123	9.497	0.27	0.1738
11	54837.1473	9.261	0.40	0.0127	10	54781.05826	9.540	0.28	0.1889
12	54959.36343	9.204	0.41	0.9698	11	54954.92647	10.147	0.37	0.8266
12	54959.37416	9.193	0.40	0.0046	11	54954.92878	10.147	0.36	0.8316
12	54959.38274	9.203	0.41	0.0324	11	54954.93449	10.153	0.35	0.8438

Table 2—Continued

Set	mJD	V	B-V ^a	Phase	Set	mJD	V	B-V ^a	Phase
12	54959.39133	9.225	0.41	0.0602	11	54954.94096	10.155	0.34	0.8577
12	54959.3952	9.238	0.41	0.0728	11	54954.94594	10.152	0.33	0.8684
12	54959.40315	9.268	0.41	0.0985	11	54954.9541	10.134	0.31	0.8858
12	54959.41578	9.315	0.42	0.1394	12	54997.46322	9.352	0.19	0.9922
13	55168.48128	9.685	0.51	0.4721	12	54997.46659	9.325	0.19	0.9994
13	55168.492	9.713	0.52	0.5068	12	54997.47241	9.298	0.18	0.0119
13	55168.50059	9.728	0.52	0.5347	12	54997.47797	9.287	0.17	0.0238
13	55168.50918	9.734	0.52	0.5625	12	54997.48304	9.289	0.16	0.0347
13	55168.51304	9.734	0.53	0.5750	12	54997.49095	9.313	0.16	0.0517
13	55168.521	9.729	0.53	0.6008	13	55176.44902	10.127	0.41	0.5980
13	55168.53225	9.712	0.53	0.6372	13	55176.45135	10.126	0.41	0.6031
					13	55176.45705	10.127	0.41	0.6153
					13	55176.46355	10.127	0.41	0.6292
					13	55176.46854	10.128	0.42	0.6399
					13	55176.4763	10.123	0.42	0.6565
					14	55341.16571	10.141	0.41	0.6220
					14	55341.16804	10.142	0.41	0.6270
					14	55341.17571	10.152	0.41	0.6435
					14	55341.18219	10.157	0.42	0.6574
					14	55341.18713	10.158	0.42	0.6680
					14	55341.193	10.162	0.42	0.6805
SU Dra					RR Lyr				
2	54396.06873	10.195	0.38	0.5930	1	49984.25103	7.68	0.38	0.417
2	54396.08065	10.195	0.38	0.6111	1	49984.25581	7.68	0.38	0.425
2	54396.09115	10.191	0.39	0.6263	1	49984.26076	7.69	0.38	0.434
2	54396.0953	10.190	0.39	0.6323	1	49984.26525	7.69	0.38	0.442
3	54426.18972	9.794	0.28	0.2019	1	49984.27176	7.7	0.38	0.453
3	54426.20164	9.826	0.30	0.2201	1	49984.27638	7.71	0.38	0.461
3	54426.21214	9.851	0.31	0.2353	4	50047.04674	7.36	0.30	0.200
3	54426.21628	9.859	0.31	0.2413	4	50047.05186	7.37	0.31	0.209
4	54478.92392	9.472	0.14	0.0514	4	50047.05669	7.39	0.32	0.218

Table 2—Continued

Set	mJD	V	B-V ^a	Phase	Set	mJD	V	B-V ^a	Phase
4	54478.93418	9.504	0.15	0.0665	4	50047.0617	7.4	0.32	0.227
4	54478.94468	9.540	0.16	0.0832	4	50047.06661	7.41	0.33	0.235
4	54478.94877	9.554	0.17	0.0892	4	50047.07193	7.43	0.34	0.245
4	54478.95101	9.562	0.17	0.0923	5	50172.97726	7.63	0.39	0.366
4	54478.96269	9.602	0.19	0.1104	5	50172.98699	7.64	0.39	0.383
4	54478.97122	9.626	0.21	0.1225	5	50172.9915	7.65	0.39	0.391
4	54478.97532	9.638	0.21	0.1286	5	50172.99797	7.66	0.38	0.402
5	54492.91603	9.852	0.31	0.2380	5	50173.00264	7.67	0.38	0.411
5	54492.92925	9.886	0.32	0.2576	6	50186.85366	7.91	0.42	0.847
5	54492.94056	9.908	0.33	0.2758	6	50186.85845	7.91	0.41	0.855
5	54492.94468	9.916	0.33	0.2819	6	50186.86339	7.93	0.40	0.864
6	54532.48479	9.701	0.24	0.1530	6	50186.86788	7.93	0.39	0.872
6	54532.49495	9.729	0.25	0.1667	6	50186.87441	7.94	0.37	0.883
6	54532.50539	9.758	0.27	0.1833	6	50186.879	7.95	0.36	0.891
6	54532.50948	9.770	0.27	0.1894	7	50201.05711	7.94	0.34	0.904
6	54532.51167	9.775	0.28	0.1939	7	50201.06191	7.93	0.33	0.913
6	54532.52188	9.804	0.29	0.2106	7	50201.06684	7.93	0.31	0.921
6	54532.53042	9.825	0.30	0.2242	7	50201.07133	7.92	0.30	0.929
6	54532.53456	9.836	0.30	0.2303	7	50201.07787	7.89	0.28	0.941
7	54586.25231	10.199	0.37	0.5666	7	50201.08245	7.86	0.27	0.949
7	54586.26252	10.207	0.38	0.5833	8	50228.80167	7.9	0.42	0.851
7	54586.27297	10.214	0.38	0.5984	8	50228.80661	7.91	0.41	0.860
7	54586.27706	10.212	0.38	0.6045	8	50228.81119	7.92	0.40	0.868
7	54586.27925	10.210	0.38	0.6075	8	50228.81616	7.93	0.38	0.876
7	54586.28946	10.206	0.39	0.6257	8	50228.8208	7.94	0.37	0.885
7	54586.298	10.203	0.39	0.6378	8	50228.82721	7.94	0.35	0.896
7	54586.30214	10.201	0.39	0.6439	9	50562.87498	7.51	0.32	0.220
8	54639.00762	10.096	0.35	0.4494	9	50562.88171	7.52	0.33	0.232
8	54639.01944	10.113	0.35	0.4660	9	50562.88664	7.53	0.34	0.241
8	54639.02994	10.126	0.36	0.4827	9	50562.89113	7.54	0.34	0.249
8	54639.03405	10.130	0.36	0.4887	9	50562.89767	7.55	0.35	0.260

Table 2—Continued

Set	mJD	V	B-V ^a	Phase	Set	mJD	V	B-V ^a	Phase
9	54733.1287	9.477	0.20	0.9667	9	50562.90226	7.56	0.36	0.268
9	54733.1406	9.477	0.20	0.9667	10	50567.58263	7.77	0.39	0.525
9	54733.1511	9.388	0.17	0.9849	10	50567.58936	7.77	0.39	0.537
9	54733.15524	9.388	0.17	0.9849	10	50567.59429	7.77	0.40	0.546
10	54833.63013	9.660	0.23	0.1446	10	50567.59878	7.78	0.40	0.554
10	54833.64205	9.697	0.25	0.1627	10	50567.60532	7.78	0.40	0.565
10	54833.65253	9.726	0.26	0.1794	10	50567.60991	7.78	0.41	0.573
10	54833.65667	9.738	0.27	0.1854	11	50745.19083	7.94	0.41	0.860
12	55130.18997	9.761	0.28	0.1935	11	50745.19752	7.95	0.39	0.872
12	55130.19992	9.791	0.29	0.2086	11	50745.20249	7.95	0.38	0.881
12	55130.2095	9.819	0.30	0.2238	11	50745.20698	7.96	0.37	0.889
12	55130.21683	9.837	0.31	0.2344	11	50745.2135	7.95	0.35	0.900
13	55143.86819	10.080	0.28	0.9046	11	50745.2181	7.94	0.33	0.908
13	55143.87203	10.005	0.28	0.9107	12	50749.22225	7.36	0.23	0.972
13	55143.87913	9.831	0.26	0.9213	12	50749.22894	7.26	0.22	0.984
13	55143.88887	9.711	0.24	0.9364	12	50749.2339	7.19	0.21	0.993
13	55143.89302	9.673	0.23	0.9425	12	50749.2384	7.13	0.17	0.001
13	55143.90014	9.585	0.22	0.9531	12	50749.24358	7.09	0.16	0.010
13	55143.90985	9.462	0.19	0.9682	12	50749.24821	7.06	0.15	0.018
13	55143.91834	9.395	0.18	0.9803	13	54781.1015	7.81	0.22	0.978
15	55149.26255	9.522	0.15	0.0737	13	54781.10757	7.73	0.21	0.989
15	55149.2725	9.556	0.17	0.0903	13	54781.11395	7.66	0.20	1.000
15	55149.28207	9.587	0.19	0.1040	13	54781.12127	7.58	0.16	0.013
15	55149.28941	9.610	0.19	0.1130	13	54781.12775	7.51	0.15	0.024
16	55317.09729	9.793	0.29	0.2067	14	54781.16808	7.4	0.17	0.095
16	55317.10911	9.824	0.30	0.2248	14	54781.17414	7.42	0.18	0.106
16	55317.11961	9.850	0.31	0.2415	14	54781.18052	7.44	0.19	0.117
16	55317.12375	9.859	0.31	0.2476	14	54781.18786	7.47	0.21	0.130
					14	54781.19433	7.49	0.22	0.142
					15	54781.36779	7.84	0.38	0.448
					15	54781.37385	7.85	0.38	0.458

Table 2—Continued

Set	mJD	V	B-V ^a	Phase	Set	mJD	V	B-V ^a	Phase
					15	54781.38023	7.86	0.38	0.470
					15	54781.38756	7.86	0.38	0.483
					15	54781.39404	7.87	0.38	0.494
					16	54782.10012	7.91	0.48	0.740
					16	54782.10618	7.91	0.48	0.750
					16	54782.11256	7.91	0.48	0.762
					16	54782.11988	7.91	0.48	0.775
					16	54782.12637	7.91	0.47	0.786
					17	54784.16409	7.78	0.39	0.381
					17	54784.17015	7.79	0.39	0.392
					17	54784.17653	7.79	0.38	0.403
					17	54784.18385	7.8	0.38	0.416
					17	54784.19034	7.81	0.38	0.427
UV Oct					VY Pyx				
1	54280.88854	9.663	0.38	0.3749	1	54391.79701	7.284	0.55	0.2171
1	54280.89363	9.677	0.38	0.3889	1	54391.80337	7.290	0.55	0.2223
1	54280.90203	9.696	0.38	0.3983	1	54391.80916	7.289	0.56	0.2269
1	54280.90706	9.708	0.38	0.4138	1	54391.81659	7.293	0.56	0.2329
2	54321.13128	9.695	0.38	0.4231	1	54391.82215	7.296	0.56	0.2374
2	54321.13642	9.697	0.44	0.6712	2	54399.99065	7.227	0.54	0.8252
2	54321.14453	9.704	0.44	0.6806	2	54399.997	7.223	0.54	0.8303
2	54321.1551	9.717	0.44	0.6956	2	54400.00278	7.222	0.54	0.8350
2	54321.16021	9.724	0.44	0.7151	2	54400.01022	7.215	0.53	0.8410
3	54371.95272	9.421	0.44	0.7245	2	54400.01578	7.212	0.53	0.8454
3	54371.95787	9.432	0.30	0.1851	3	54406.38762	7.194	0.51	0.9842
3	54371.96595	9.451	0.31	0.1945	3	54406.39397	7.194	0.51	0.9893
3	54371.97653	9.476	0.32	0.2094	3	54406.39975	7.194	0.50	0.9940
3	54371.98163	9.488	0.33	0.2289	3	54406.40719	7.194	0.50	0.0000
4	54376.00938	9.648	0.34	0.2383	3	54406.41275	7.197	0.50	0.0045
4	54376.01451	9.662	0.44	0.6945	4	54414.18113	7.313	0.57	0.2695
4	54376.0226	9.689	0.44	0.7040	4	54414.18749	7.315	0.57	0.2747

Table 2—Continued

Set	mJD	V	B-V ^a	Phase	Set	mJD	V	B-V ^a	Phase
4	54376.03318	9.727	0.44	0.7189	4	54414.19328	7.318	0.57	0.2793
4	54376.0383	9.745	0.43	0.7384	4	54414.20071	7.321	0.57	0.2853
5	54522.69065	9.172	0.43	0.7479	4	54414.20626	7.323	0.57	0.2898
5	54522.69579	9.185	0.16	0.0250	5	54421.04014	7.242	0.55	0.8012
5	54522.70389	9.208	0.16	0.0344	5	54421.04649	7.237	0.54	0.8063
5	54522.71447	9.233	0.17	0.0494	5	54421.05229	7.235	0.54	0.8110
5	54522.71955	9.243	0.19	0.0689	5	54421.05972	7.228	0.54	0.8170
6	54551.36091	9.377	0.20	0.0782	5	54421.06527	7.227	0.54	0.8215
6	54551.36606	9.243	0.34	0.8636	6	54427.69953	7.266	0.54	0.1719
6	54551.37417	9.033	0.33	0.8731	6	54427.70588	7.268	0.54	0.1770
6	54551.38473	8.868	0.31	0.8881	6	54427.71167	7.269	0.54	0.1817
6	54551.38984	8.834	0.29	0.9075	6	54427.7191	7.273	0.54	0.1877
7	54569.72058	9.757	0.28	0.9169	6	54427.72465	7.276	0.54	0.1922
7	54569.72574	9.762	0.44	0.7001	7	54439.55301	7.300	0.57	0.7315
7	54569.73384	9.778	0.44	0.7096	7	54439.55938	7.297	0.57	0.7367
7	54569.74442	9.797	0.44	0.7245	7	54439.56516	7.293	0.56	0.7413
7	54569.74951	9.806	0.43	0.7440	7	54439.57259	7.286	0.56	0.7473
8	54601.98409	9.356	0.43	0.7534	7	54439.57815	7.284	0.56	0.7518
8	54601.98925	9.368	0.28	0.1610	8	54458.27282	7.213	0.54	0.8287
8	54601.99733	9.390	0.29	0.1706	8	54458.2792	7.209	0.54	0.8339
8	54602.00791	9.418	0.30	0.1854	8	54458.28498	7.205	0.54	0.8385
8	54602.01302	9.430	0.31	0.2049	8	54458.29241	7.202	0.53	0.8445
9	54660.78087	9.629	0.32	0.2144	8	54458.29796	7.200	0.53	0.8490
9	54660.78602	9.629	0.40	0.5222	9	54466.59728	7.424	0.60	0.5423
9	54660.79411	9.630	0.40	0.5317	9	54466.60366	7.423	0.60	0.5474
9	54660.80468	9.635	0.41	0.5466	9	54466.60944	7.424	0.60	0.5521
9	54660.80979	9.639	0.41	0.5661	9	54466.61686	7.423	0.60	0.5581
10	54704.02235	9.446	0.42	0.5755	9	54466.62242	7.421	0.60	0.5625
10	54704.02749	9.458	0.32	0.2153	10	54471.59201	7.416	0.60	0.5704
10	54704.03559	9.479	0.33	0.2248	10	54471.59838	7.413	0.60	0.5756
10	54704.04617	9.508	0.34	0.2397	10	54471.60417	7.413	0.60	0.5802

Table 2—Continued

Set	mJD	V	B-V ^a	Phase	Set	mJD	V	B-V ^a	Phase
10	54704.05126	9.523	0.35	0.2592	10	54471.61116	7.410	0.60	0.5862
11	54900.0444	9.714	0.35	0.2686	10	54471.61716	7.408	0.60	0.5907
11	54900.04955	9.717	0.39	0.4797	11	54482.71326	7.412	0.60	0.5395
11	54900.05764	9.719	0.39	0.4892	11	54482.71963	7.412	0.60	0.5447
11	54900.06822	9.724	0.40	0.5041	11	54482.72542	7.411	0.60	0.5493
11	54900.07331	9.727	0.40	0.5236	11	54482.73285	7.411	0.60	0.5553
12	54908.69757	9.660	0.40	0.5330	11	54482.7384	7.406	0.60	0.5598
12	54908.70125	9.662	0.38	0.4273	12	54491.30479	7.406	0.60	0.4685
12	54908.70933	9.668	0.38	0.4341	12	54491.31115	7.405	0.60	0.4736
12	54908.71991	9.670	0.39	0.4490	12	54491.31693	7.408	0.61	0.4782
12	54908.725	9.671	0.39	0.4685	12	54491.32436	7.409	0.61	0.4842
13	55075.29118	9.626	0.39	0.4779	12	54491.32993	7.411	0.61	0.4887
13	55075.29632	9.628	0.39	0.4557	13	54499.62819	7.271	0.54	0.1811
13	55075.30442	9.631	0.39	0.4652	13	54499.63456	7.272	0.54	0.1863
13	55075.315	9.637	0.39	0.4801	13	54499.64035	7.273	0.54	0.1909
13	55075.32008	9.640	0.40	0.4996	13	54499.64778	7.275	0.55	0.1969
14	55087.85755	9.681	0.40	0.5090	13	54499.65333	7.277	0.55	0.2014
14	55087.86269	9.682	0.43	0.6153	14	54526.47303	7.217	0.54	0.8310
14	55087.87078	9.696	0.43	0.6247	14	54526.47941	7.215	0.54	0.8362
14	55087.88135	9.725	0.43	0.6396	14	54526.48519	7.212	0.53	0.8408
14	55087.88646	9.740	0.44	0.6591	14	54526.49262	7.208	0.53	0.8468
15	55148.83507	9.040	0.44	0.6685	14	54526.49818	7.207	0.53	0.8513
15	55148.84021	9.066	0.18	0.9955	15	54532.39944	7.395	0.60	0.6106
15	55148.8483	9.110	0.15	0.0050	15	54532.40581	7.392	0.59	0.6157
15	55148.85888	9.161	0.16	0.0199	15	54532.4116	7.384	0.59	0.6204
15	55148.86398	9.183	0.17	0.0394	15	54532.41903	7.381	0.59	0.6264
					15	54532.42458	7.380	0.59	0.6309
					16	54799.06059	7.353	0.58	0.6682
					16	54799.06696	7.351	0.58	0.6733
					16	54799.07274	7.347	0.58	0.6780
					16	54799.08017	7.340	0.58	0.6840

Table 2—Continued

Set	mJD	V	B-V ^a	Phase	Set	mJD	V	B-V ^a	Phase
					16	54799.08573	7.338	0.58	0.6885
					17	54817.77185	7.279	0.56	0.7585
					17	54817.77822	7.272	0.56	0.7636
					17	54817.784	7.268	0.56	0.7683
					17	54817.79144	7.265	0.55	0.7743
					17	54817.79699	7.260	0.55	0.7788
					18	54860.52883	7.285	0.56	0.2413
					18	54860.53521	7.287	0.56	0.2464
					18	54860.541	7.292	0.56	0.2511
					18	54860.54843	7.297	0.56	0.2571
					18	54860.55398	7.298	0.57	0.2616
					19	55289.58789	7.310	0.57	0.2700
					19	55289.59426	7.309	0.57	0.2752
					19	55289.60003	7.314	0.57	0.2798
					19	55289.60747	7.318	0.57	0.2858
					19	55289.61303	7.318	0.57	0.2903
					20	55301.43772	7.222	0.54	0.8267
					20	55301.44407	7.218	0.54	0.8318
					20	55301.44985	7.215	0.54	0.8365
					20	55301.45728	7.211	0.53	0.8425
					20	55301.46285	7.207	0.53	0.8470
					21	55325.93291	7.409	0.60	0.5816
					21	55325.93927	7.408	0.60	0.5868
					21	55325.94506	7.406	0.60	0.5914
					21	55325.95249	7.404	0.60	0.5974
					21	55325.95804	7.403	0.60	0.6019
					22	55332.25647	7.344	0.58	0.6815
					22	55332.26284	7.341	0.58	0.6866
					22	55332.26862	7.339	0.58	0.6913
					22	55332.27605	7.334	0.58	0.6973
					22	55332.28161	7.331	0.58	0.7018

Table 2—Continued

Set	mJD	V	B-V ^a	Phase	Set	mJD	V	B-V ^a	Phase
					23	55351.36845	7.227	0.52	0.0950
					23	55351.37481	7.229	0.52	0.1001
					23	55351.3806	7.230	0.52	0.1048
					23	55351.38803	7.231	0.52	0.1108
					23	55351.39359	7.234	0.52	0.1152
κ Pav									
1	54280.81179	4.207	0.60	0.1921					
1	54280.82106	4.210	0.61	0.1931					
1	54280.82566	4.212	0.61	0.1936					
1	54280.83559	4.212	0.61	0.1947					
2	54321.05596	4.633	0.86	0.6235					
2	54321.06751	4.634	0.86	0.6248					
2	54321.07611	4.631	0.86	0.6258					
2	54321.08404	4.633	0.86	0.6266					
2	54321.09235	4.633	0.86	0.6276					
2	54321.10119	4.631	0.86	0.6285					
3	54373.07462	4.472	0.82	0.3516					
3	54373.08557	4.474	0.82	0.3528					
3	54373.09296	4.475	0.83	0.3536					
3	54373.1042	4.477	0.83	0.3548					
3	54373.11263	4.480	0.83	0.3558					
3	54373.12443	4.482	0.83	0.3571					
4	54519.03565	4.569	0.89	0.4241					
4	54519.04564	4.571	0.89	0.4252					
4	54519.05097	4.572	0.89	0.4258					
4	54519.06171	4.575	0.89	0.4270					
5	54548.08718	4.662	0.86	0.6231					
5	54548.09788	4.660	0.86	0.6243					
5	54548.10277	4.659	0.86	0.6248					
5	54548.11111	4.660	0.86	0.6258					
5	54548.11814	4.660	0.86	0.6265					

Table 2—Continued

Set	mJD	V	B-V ^a	Phase	Set	mJD	V	B-V ^a	Phase
5	54548.12516	4.657	0.86	0.6273					
7	54601.02693	4.613	0.90	0.4526					
7	54601.03856	4.614	0.90	0.4539					
7	54601.04464	4.613	0.90	0.4545					
7	54601.05392	4.612	0.90	0.4556					
7	54601.06093	4.612	0.90	0.4563					
7	54601.06792	4.617	0.90	0.4571					
8	54653.05113	4.192	0.59	0.1813					
8	54653.06206	4.196	0.59	0.1825					
8	54653.06906	4.196	0.59	0.1832					
8	54653.0803	4.196	0.59	0.1845					
8	54653.08878	4.201	0.59	0.1854					
8	54653.10058	4.203	0.60	0.1867					
9	54659.04949	4.219	0.57	0.8418					
9	54659.06061	4.215	0.57	0.8430					
9	54659.06693	4.211	0.57	0.8437					
9	54659.07627	4.205	0.57	0.8447					
10	54705.88251	3.965	0.42	0.9988					
10	54705.89347	3.963	0.42	1.0000					
10	54705.9005	3.963	0.42	0.0008					
10	54705.9117	3.963	0.42	0.0020					
10	54705.92017	3.963	0.42	0.0029					
10	54705.93197	3.961	0.42	0.0042					
12	54877.21429	4.102	0.54	0.8650					
12	54877.22524	4.097	0.54	0.8662					
12	54877.23265	4.094	0.54	0.8670					
12	54877.24388	4.089	0.54	0.8683					
12	54877.25233	4.083	0.54	0.8692					
12	54877.26414	4.078	0.53	0.8705					
13	54986.28763	4.078	0.53	0.8757					
13	54986.30008	4.074	0.52	0.8770					

Table 2—Continued

Set	mJD	V	B-V ^a	Phase	Set	mJD	V	B-V ^a	Phase
13	54986.30903	4.069	0.52	0.8780					
13	54986.32178	4.064	0.52	0.8794					
13	54986.33166	4.064	0.52	0.8805					
13	54986.34207	4.061	0.52	0.8816					
14	55093.89644	4.596	0.75	0.7250					
14	55093.90741	4.596	0.74	0.7262					
14	55093.91481	4.596	0.74	0.7270					
14	55093.92604	4.594	0.74	0.7283					
14	55093.93447	4.593	0.74	0.7292					
14	55093.94627	4.594	0.74	0.7305					
15	55148.88147	4.531	0.67	0.7797					
15	55148.8887	4.529	0.67	0.7805					
15	55148.89303	4.527	0.66	0.7810					
15	55148.89762	4.524	0.66	0.7815					
15	55148.90877	4.523	0.66	0.7827					
15	55148.9153	4.523	0.66	0.7834					
15	55148.92083	4.522	0.66	0.7840					
15	55148.92597	4.521	0.66	0.7846					

^aB-V estimated from phased light curve.

Table 3. Reference Stars: Visible and Near-IR Photometry

FGS ID	PPMXL ID	V	B-V	K ^a	J-K	V-K
XZ Cyg						
2	178627907000819000	15.24	0.79±0.11	13.34	0.45	1.90
3	178627800678871000	15.00	0.72 0.1	13.30	0.37	1.70
4	178627507943789000	12.55	1.26 0.03	9.51	0.84	3.04
5	178626897495064000	13.16	0.50 0.04	11.96	0.30	1.20
6	178627902818755000	12.46	0.65 0.03	11.03	0.37	1.43
UV Oct						
9	6050827457780530000	15.92	0.68 0.04	14.25	0.41	1.67
10	6050827543215700000	15.35	0.94 0.05	13.01	0.57	2.35
11	6050827517824970000	14.91	0.63 0.04	13.24	0.40	1.67
12	6050827495380950000	13.12	1.35 0.03	9.82	0.87	3.30
13	6050827141173300000	14.45	0.63 0.04	12.74	0.38	1.71
RZ Cep						
17	236149611067714000	14.90	1.09 0.07	12.26	0.56	2.64
18	236150055842444000	16.30	1.29 0.15	13.04	0.60	3.26
19	236150360634453000	16.16	0.96 0.15	13.32	0.75	2.84
20	236150404085559000	15.31	1.25 0.1	12.52	0.69	2.79
21	236149242851448000	14.06	1.00 0.06	11.74	0.50	2.32
22	236150379961202000	12.52	0.62 0.03	11.01	0.29	1.51
SU Dra						
24	910626741647084000	16.26	0.70 0.12	14.51	0.39	1.76
25	910625310986521000	13.10	0.47 0.04	11.80	0.32	1.30
26	910625114428228000	14.60	1.17 0.06	12.14	0.59	2.46
27	910626124371472000	14.36	0.64 0.05	12.66	0.41	1.70
28	910627013779397000	15.19	0.54 0.09	13.75	0.36	1.44
κ Pav						
31	6417195936484110000	12.65	1.17 0.03	9.98	0.68	2.67
32	6417195914995010000	14.24	0.70 0.05	12.56	0.42	1.68
33	6417196083800320000	14.55	0.93 0.04	12.39	0.49	2.17
34	6417197688468440000	15.94	0.95 0.06	13.72	0.51	2.22
35	6417383894358280000	14.84	0.85 0.04	12.96	0.48	1.88

Table 3—Continued

FGS ID	PPMXL ID	V	B-V	K ^a	J-K	V-K
36	6417383768816120000	15.31	0.88 0.05	13.30	0.53	2.01
37	6417197455800920000	15.7	0.89 0.1	13.74	0.45	1.96
VY Pyx						
39	1264343482 ^b	12.45	1.34 0.03	9.08	0.89	3.37
40	2735010192495240000	15.31	0.55 0.09	13.77	0.32	1.54
41	1264343537 ^b	15.30	0.93 0.09	13.08	0.53	2.22
42	2735033696661810000	14.41	0.62 0.05	12.71	0.39	1.70
43	2735057261695820000	16.15	0.52 0.15	14.66	0.29	1.49

^aJ, K from 2MASS catalog

^bID from 2MASS catalog

Table 4. Astrometric Reference Star Spectrophotometric Parallaxes

ID	V	Sp. T.	M_V	A_V	m-M	π_{abs} (mas)
XZ Cyg						
2	15.24	K0V	5.9	0.0	9.34±0.5	1.3±0.3
3	15	G1.5V	4.6	0.3	10.39 0.5	1.0 0.2
4	12.55	K2III	0.5	0.3	12.05 0.5	0.5 0.1
5	13.16	F7V	3.9	0.0	9.3 0.5	1.4 0.3
6	12.46	G2V	4.7	0.0	7.78 0.5	2.8 0.6
UV Oct						
9	15.92	G5V	5.1	0.1	10.8 0.5	0.7 0.2
10	15.35	K0V	5.9	0.4	9.5 0.5	1.6 0.4
11	14.91	G0V	4.2	0.2	10.7 0.5	0.8 0.2
12	13.12	K3III	0.3	0.3	12.8 0.5	0.3 0.1
13	14.45	F9V	4.2	0.2	10.2 0.5	1.0 0.2
RZ Cep						
17	14.9	G1V	4.5	1.4	10.36 0.5	1.6 0.4
18	16.3	G1V	4.5	2.1	11.76 0.5	1.2 0.3
19	16.16	G2V	4.7	1.3	11.48 0.5	0.9 0.2
20	15.31	K0V	5.9	1.1	9.41 0.5	2.2 0.5
21	14.06	G1V	4.5	1.1	9.52 0.5	2.1 0.5
22	12.52	A1V	0.9	1.7	11.61 0.5	1.1 0.2
SU Dra						
24	16.26	G5V	5.1	0.1	11.16 0.5	0.6 0.1
25	13.1	F6V	3.7	0.1	9.42 0.5	1.4 0.3
26	14.6	K2.5V	6.6	0.4	7.97 0.5	3.0 0.7
27	14.36	G5V	5.1	0.0	9.26 0.5	1.4 0.3
28	15.19	F9V	4.2	0.0	10.97 0.5	0.7 0.1
κ Pav						
31	12.65	K1.5III	0.6	0.1	12.1 0.5	0.4 0.1

Table 4—Continued

ID	V	Sp. T.	M_V	A_V	m-M	$\pi_{abs}(\text{mas})$
32	14.24	G3V	4.8	0.2	9.4 0.5	1.4 0.3
33	14.55	K1V	6.2	0.1	8.4 0.5	2.2 0.5
34	15.94	K1V	6.2	0.2	9.8 0.5	1.2 0.3
35	14.84	K0V	5.9	0.0	8.9 0.5	1.6 0.4
36	15.31	K0V	5.9	0.1	9.4 0.5	1.4 0.3
37	15.7	K0V	5.9	0.1	9.8 1.0	1.2 0.5
VY Pyx						
39	12.45	K3III	0.3	0.3	12.15 0.5	0.4 0.1
40	15.31	F4V	3.3	0.5	11.97 0.5	0.5 0.1
41	15.30	G8V	5.6	0.5	9.72 0.5	1.4 0.3
42	14.41	F6V	3.7	0.5	10.73 0.5	0.9 0.2
43	16.15	F4V	3.3	0.4	12.81 0.5	0.3 0.1

Table 5. κ Pav and Reference Star Relative Positions ^a

FGS ID	V	ξ ^b	η ^b
κ Pav	4.23	-57.7608 \pm 0.0002	-156.2033 \pm 0.0002
31	12.65	-75.1709 0.0010	-47.2432 0.0012
32 ^c	14.23	0.0000 0.0003	0.0000 0.0003
33	14.53	-150.7073 0.0003	-195.2863 0.0003
34	15.81	48.7661 0.0007	-151.6338 0.0010
35	14.84	-70.5595 0.0004	-298.9709 0.0004
36	15.3	-149.3689 0.0003	-278.0559 0.0003
37	15.68	38.8649 0.0004	-59.3234 0.0005

^aepoch 2007.744

^b ξ and η are relative positions in arcseconds

^cRA = 284°230996, Dec = -67°187251, J2000, epoch 2007.744

Table 6. κ Pav and Reference Star Relative Proper Motion, Parallax and Space Velocity

ID	μ_x^a	μ_y^a	π_{abs}^b	V_t^c
κ Pav ^d	-7.41±0.24	16.41±0.24	5.57±0.28	15.3±0.9
31	3.38 0.23	-4.79 0.22	1.82 0.25	15.2 2.5
32	29.47 0.73	-0.26 0.97	1.16 0.42	120.9 443.4
33	0.89 0.33	-0.28 0.35	0.17 0.27	25.2 51.5
34	-0.11 0.50	-15.51 0.44	0.26 0.42	280 1311
35	-8.80 1.15	-3.04 1.03	1.74 0.42	25.4 11.1
36	-9.79 0.39	-3.55 0.42	1.15 0.34	42.8 13.7
37	9.80 0.49	-3.31 0.44	1.46 0.33	33.5 8.9

^a μ_x and μ_y are relative motions along RA and Dec in mas yr⁻¹

^bParallax in mas

^c $V_t = 4.74 \times \mu / \pi_{abs}$

^dModeled with equations 2 – 5

Table 7. CP2 Parallaxes, Proper Motions, and Absolute Magnitudes

Parameter		
	κ Pav	VY Pyx
Duration (y)	2.23	2.63
Ref stars (#)	7	5
Ref $\langle V \rangle$	14.75	14.72
Ref $\langle B-V \rangle$	0.91	0.79
<i>HST</i> μ (mas y ⁻¹)	18.1±0.1	31.8±0.2
P.A. (°)	335.5±0.1	20.5±0.1
V_t^a (km s ⁻¹)	16.0±0.7	23.4±0.6
<i>HST</i> π_{abs} (mas)	5.57 ± 0.28	6.44 ± 0.23
Hip97 π_{abs} (mas)	6.00±0.67	5.74±0.76
Hip07 π_{abs} (mas)	6.52±0.77	5.01±0.44
LKH Corr	-0.02	-0.01
(m-M) ₀	6.29	6.00
M _V	-1.99±0.11	+1.18±0.08
M _K	-3.52±0.11	-0.26±0.08

$$^a V_t = 4.74 \times \mu / \pi_{abs}$$

Table 8. RRL Parallaxes, Proper Motions, and Absolute Magnitudes

Parameter					
	XZ Cyg	UV Oct	RZ Cep	SU Dra	RR Lyr
Duration (y)	2.87	2.38	2.41	2.52	13.14
Ref stars (#)	4	5	4	5	5
Ref $\langle V \rangle$	13.68	14.75	14.88	14.70	13.75
Ref $\langle B-V \rangle$	0.78	0.85	1.04	0.70	0.71
<i>HST</i> μ (mas y ⁻¹)	86.1±0.1	133.4±0.2	214.4±0.3	90.7±0.2	222.5±0.1
P.A. (°)	106.3±0.2	205.8±0.1	25.4±0.1	210.9±0.1	209.1±0.1
V_t^a (km s ⁻¹)	245±22	368±20	400±27	307±25	333±13
<i>HST</i> π_{abs} (mas)	1.67 ± 0.17	1.71 ± 0.10	2.12 ± 0.16	1.42 ± 0.16	3.77 ± 0.13
Hip97 π_{abs} (mas)	2.28±0.86	1.48±0.94	0.22±1.09	1.11±1.15	4.38±0.59
Hip07 π_{abs} (mas)	2.29±0.84	2.44±0.81	0.59±1.48	0.20±1.13	3.46±0.64
LKH Corr	-0.09	-0.03	-0.05	-0.11	-0.02
(m-M) ₀	8.99	8.85	8.02	9.38	7.13
M_V	+0.41±0.22	+0.35±0.13	+0.27±0.17	+0.40±0.25	+0.54±0.07
M_K	-0.29±0.22	-0.60±0.13	-0.40±0.16	-0.73±0.25	-0.65±0.07

^aTangential velocity, $V_t = 4.74 \times \mu / \pi_{abs}$

Table 9. K and V Zero-Points, a_n

n	λ	a(LKH)		a(RP)		b ¹	c ²	Notes
1	K _s	-0.56±0.02		-0.54±0.03		-2.38	0.08	Sollima et al. (2008)
2	K _s	-0.57	0.03	-0.54	0.03	-2.38	-	Sollima et al. (2006), no [Fe/H]
3	K _s	-0.58	0.04	-0.56	0.04	-2.101	0.231	Bono et al. (2003)
4	K _s	-0.56	0.02	-0.53	0.04	-2.16	-	Dall’Ora et al. (2004)
5	K _s	-0.57	0.02	-0.53	0.03	-2.71	0.12	Del Principe et al. (2006)
6	K _s	-0.56	0.03	-0.54	0.03	-2.11	0.05	Borissova et al. (2009)
7	V	0.45	0.05	0.46	0.03	-	0.214	Gratton et al. (2004)

¹b = log P coefficient

²c = [Fe/H] coefficient

Table 10. RRL M_V at $[\text{Fe}/\text{H}]=-1.5$

M_V	Source ^a
0.45±0.05	TP, this study, LKH
0.46 0.03	TP, this study, RP
0.40 0.22	TP, Koen & Laney (1998)
0.61 0.16 ^b	TP, Benedict <i>et al.</i> (2002a,b), Feast (2002)
0.47 0.12	GC, Carretta <i>et al.</i> (2000)
0.62 0.11	HB, Carretta <i>et al.</i> (2000)
0.75 0.13	SP, Gould & Popowski (1998)
0.55 0.12	SB, Cacciari & Clementini (2003)
0.68 0.05	SP, Fernley <i>et al.</i> (1998a)

^aSP = statistical parallax, GC = from subdwarf fits to globular clusters, HB = from trig parallax of field HB stars, SB = surface brightness, TP = trig parallax

^bBased on RR Lyrae only; includes an estimated cosmic dispersion component

Table 11. Globular Cluster Distance Moduli and Ages

ID	[Fe/H] ^a	E(B-V)	λ	m_0	M_0	$(m-M)_0$	Ref. ^b	Age ^c
M3	-1.57	0.01	V	15.62±0.05	0.45±0.11	15.17±0.12	1	
			K_s	13.93 0.04	-1.23 ^d	15.16 0.06	2	10.8±1.0
M4	-1.40	0.36	V	12.15 0.06	0.47 0.12	11.68 0.13	3	
			K_s	10.97 0.06	-0.52	11.48 0.08	4	11.1 ^{-1.4} _{+1.7}
M15	-2.16	0.09	V	15.51 0.05	0.32 0.08	15.20 0.09	5	
			K_s	14.67 0.1	-0.52	15.18 0.11	4	12.1 1.0
M68	-2.08	0.04	V	15.51 0.01	0.33 0.08	15.18 0.08	6	
			K_s	14.35 0.04	-0.75	15.10 0.06	7	12.4 1.0
ω Cen	-1.84	0.11	V	14.2 0.02	0.38 0.09	13.82 0.09	8	
			K_s	13.05 0.06	-0.75	13.80 0.08	9	–
M92	-2.16	0.025	V	15.01 0.08	0.31 0.08	14.70 0.11	10	
			K_s	13.86 0.04	-0.78	14.64 0.06	11	13.1 1.1

^aZW scale

^b1 Benkő et al. (2006); 2 Butler (2003); 3 Cacciari (1979); 4 Longmore et al. (1990), $\langle K \rangle$ and error estimated from figure 1(c) at $\log P = -0.3$; 5 Silbermann & Smith (1995), table 6, RRL ab only; 6 Walker (1994); 7 Dall’Ora et al. (2006); 8 Olech et al. (2003); 9 Del Principe et al. (2006), $\log P = -0.2$; 10 Kopacki (2001), table2, intensity averaged V; 11 Del Principe et al. (2005), table 3, RRL ab only, $\langle \log P \rangle = -0.19$.

^cin Gy

^d M_K errors, $\sigma = 0.05$ mag

Table 12. LMC Distance Moduli

Bandpass	(m-M) ₀	Source
RRL		
K _s	18.55±0.05	1
V	18.61 0.05	2
V	18.46 0.06	3
Reticulum Cluster RRL		
K _s	18.50 0.03	4
Classical Cepheids		
V	18.52 0.06	5
K	18.48 0.04	5
W _{VI}	18.51 0.04	5

Notes:

1 LMC data from Borissova et al. (2009)

2 LMC data from Gratton et al. (2004)

3 LMC data from Soszynski et al. (2003)

4 Reticulum cluster data from Dall’Ora et al. (2004)

5 See Benedict et al. (2007)

The results for both the RRs and Cepheids are from LKH corrected absolute magnitudes.

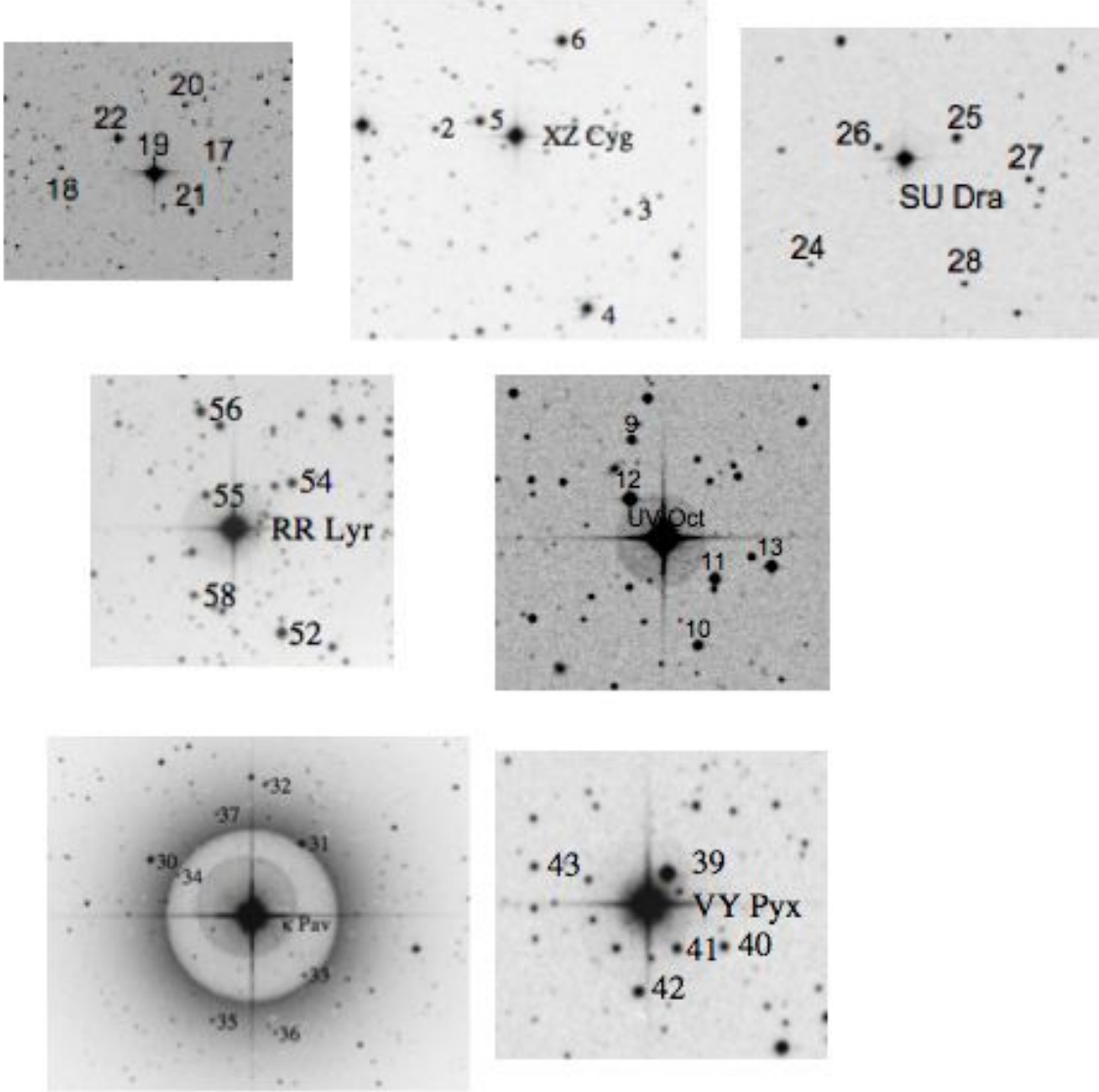


Fig. 1.— The RRL and CP2 fields with astrometric reference stars marked. Boxes are roughly $2'$ across with North to the top, East to the left. RZ Cep is at top left.

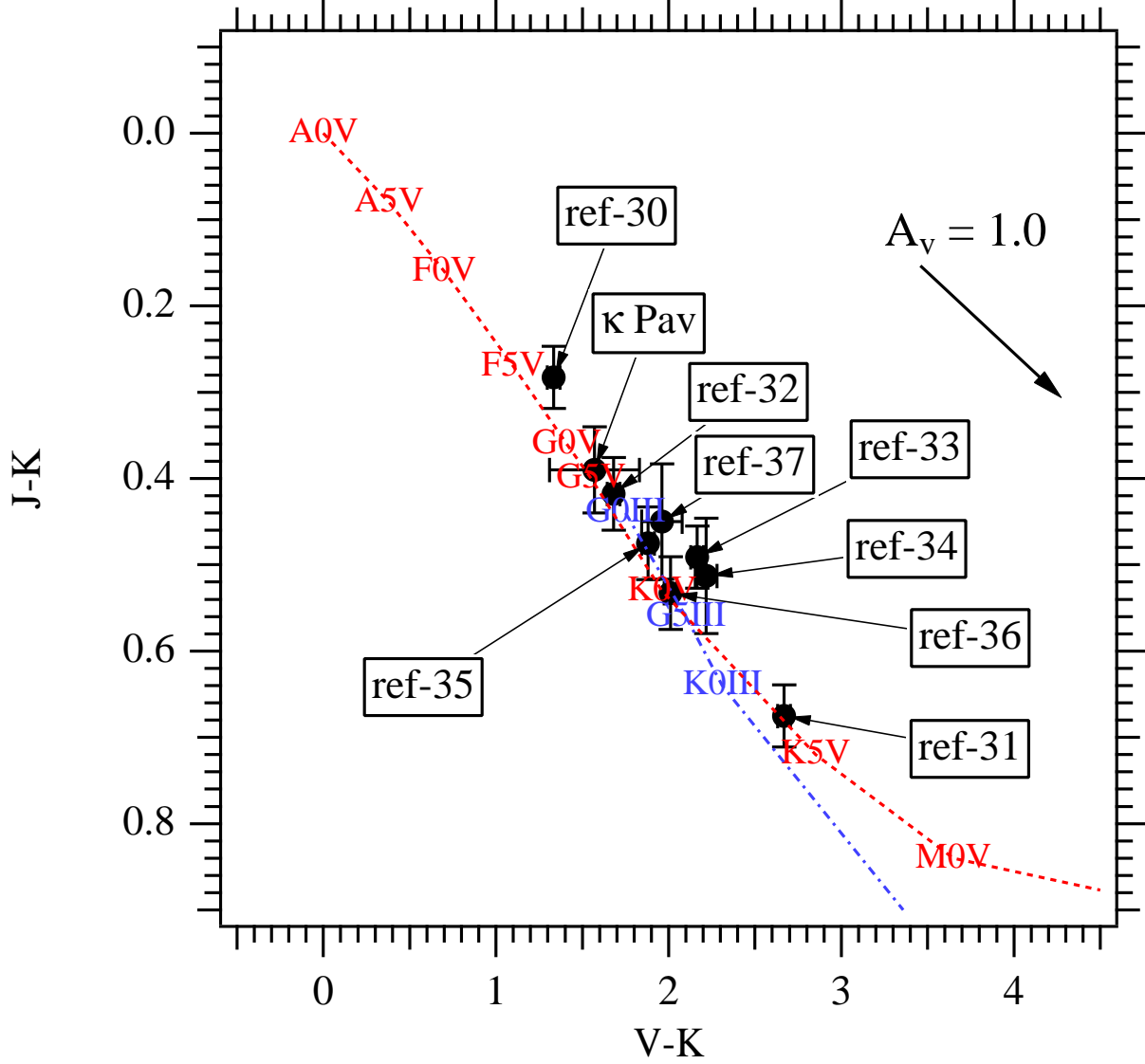


Fig. 2.— J-K vs V-K color-color diagram for κ Pav and reference stars. The dashed line is the locus of dwarf (luminosity class V) stars of various spectral types; the dot-dashed line is for giants (luminosity class III). The reddening vector indicates $A_V=1.0$ for the plotted color systems. For this field at Galactic latitude $\ell^{II} = -25^\circ$, $\langle A_V \rangle = 0.05 \pm 0.06$ magnitude (Table 4) with a maximum of 0.22 (Schlegel et al. 1998).

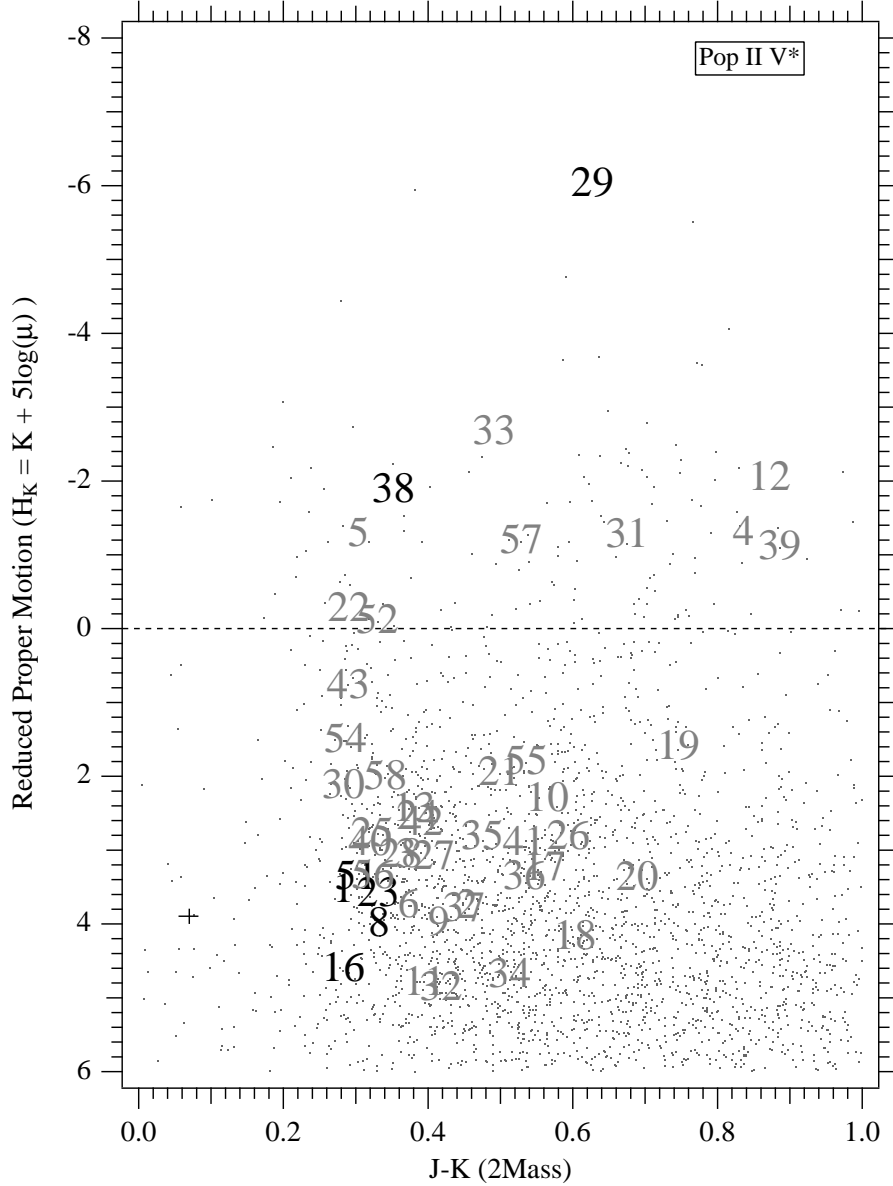


Fig. 3.— Reduced proper motion diagram for 4039 stars taken from $\frac{1}{3}^\circ \times \frac{1}{3}^\circ$ fields centered on each variable star. Star identifications are shown (black) for XZ Cyg (1), UV Oct (8), RZ Cep (16), SU Dra (23), κ Pav (29), VY Pyx (38), RR Lyr (51), and for (grey) all astrometric reference stars in Table 4. Ref-52 through -58 are from Benedict et al. (2002b). H_K for all numbered stars is calculated using our final proper motions, examples of which for the κ Pav field can be found in Table 6. For a given spectral type giants and sub-giants have more negative H_K values and are redder than dwarfs in J-K. Reference stars ref-4, -12, -31, -39 are confirmed giants. The plotted position (but not the colors from Table 3) suggests a sub-giant classification for ref-33. The cross in the lower left corner indicates representative internal errors along each axis.

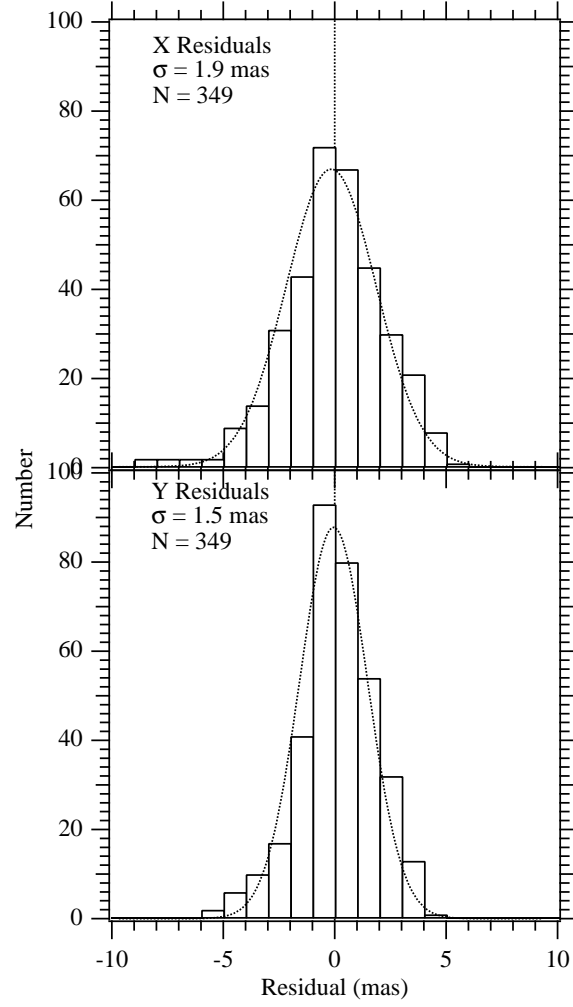


Fig. 4.— Histograms of x and y residuals obtained from modeling κ Pav and astrometric reference stars with equations 4 and 5, constraining $D=-B$ and $E=A$. Distributions are fit with gaussians whose $1-\sigma$ dispersions are noted in the plots.

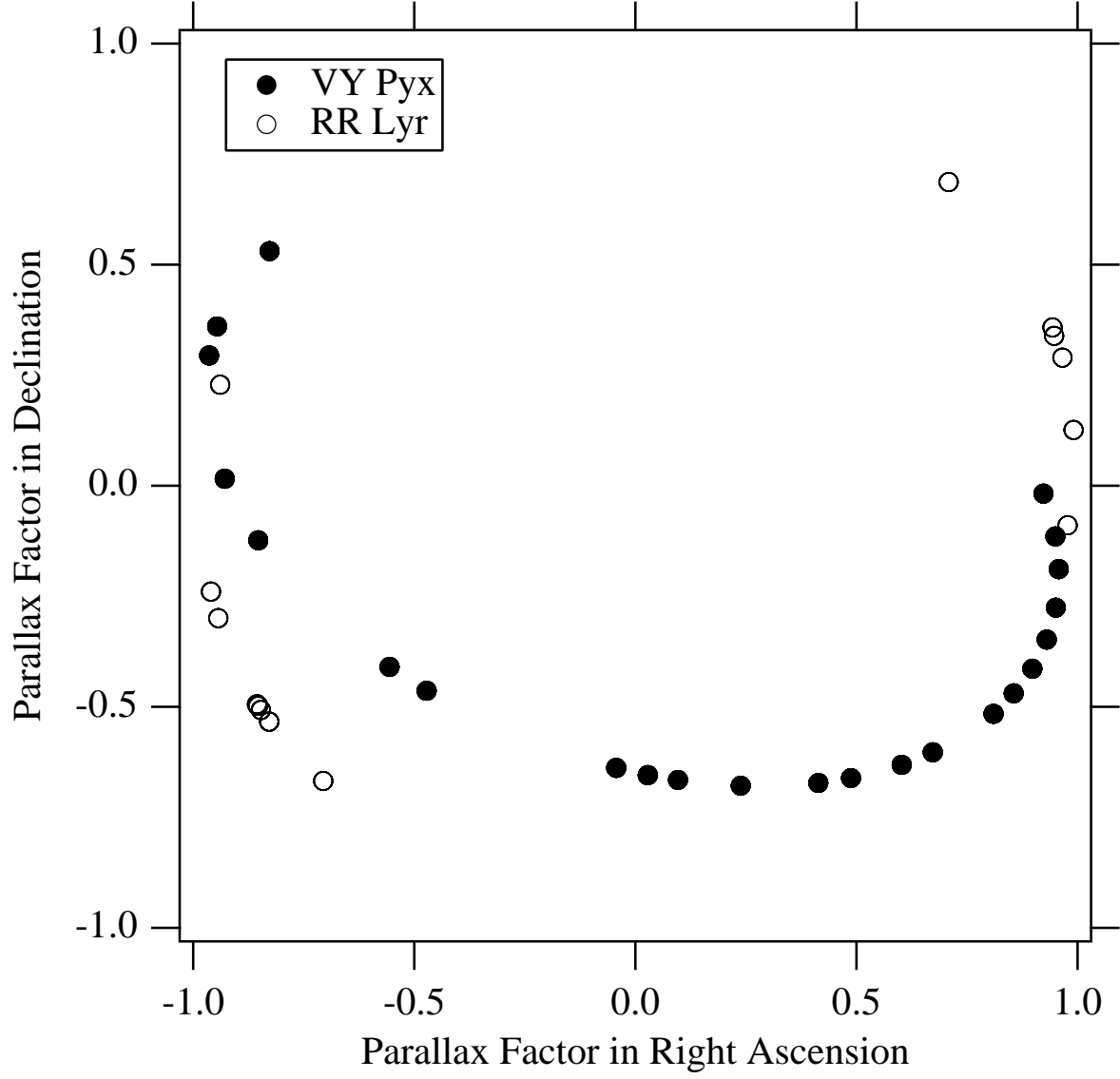


Fig. 5.— Sampling of the parallactic ellipses of VY Pyx and RR Lyr. Lack of coverage is not an issue in the parallax of VY Pyx.

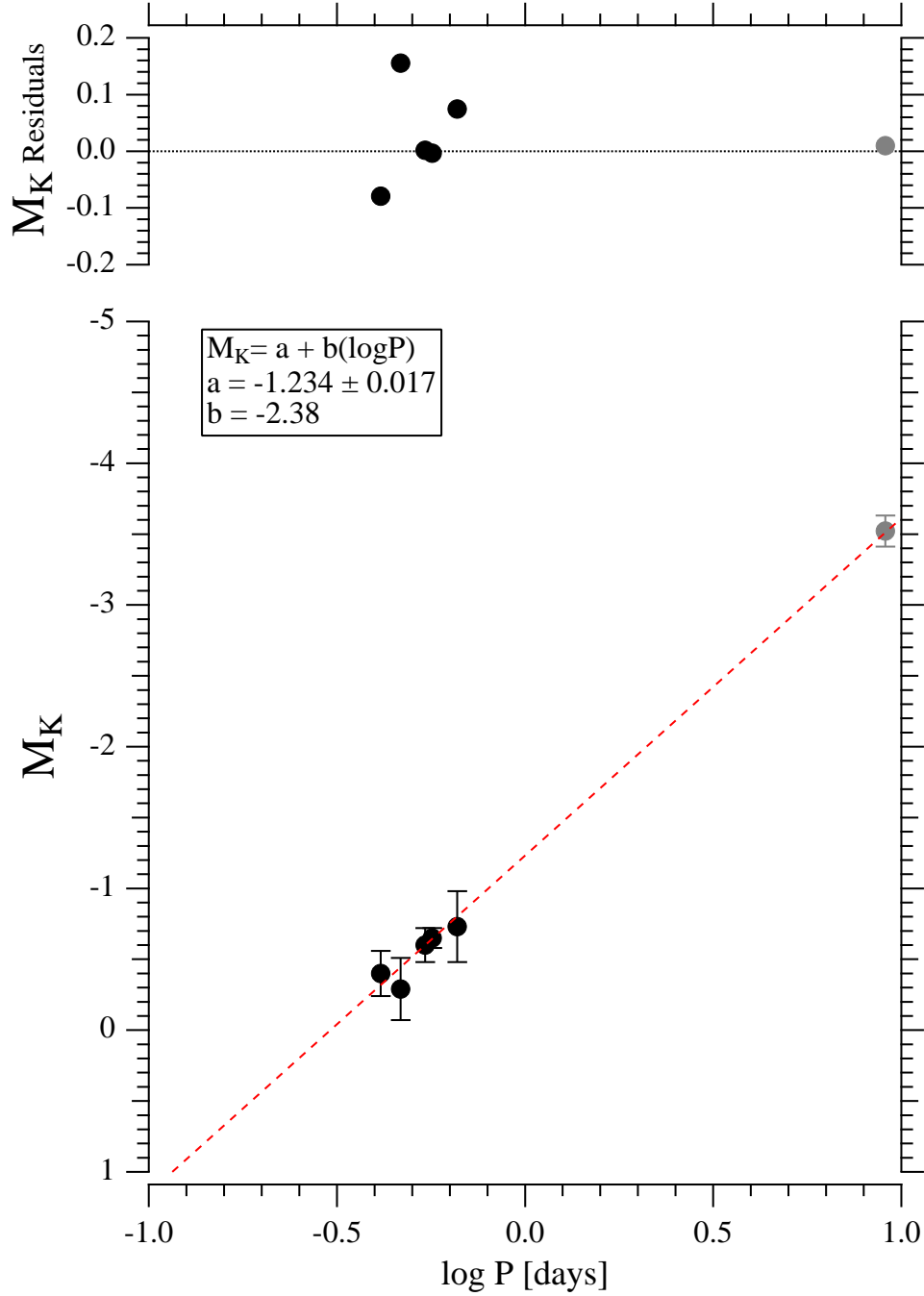


Fig. 6.— A Pop II K-band PLR. All magnitudes have been corrected for interstellar extinction. Coefficients are for $M_K = a + b * (\log P)$. Zero-point (a) error is 1σ . The absolute magnitude (uncorrected for ‘peculiarity’) and residual for $\kappa \text{ Pav}$ are plotted in grey. The fit is without $\kappa \text{ Pav}$. The slope is constrained to $b=-2.38$ (Sollima et al. 2006). The largest residual is for XZ Cyg.

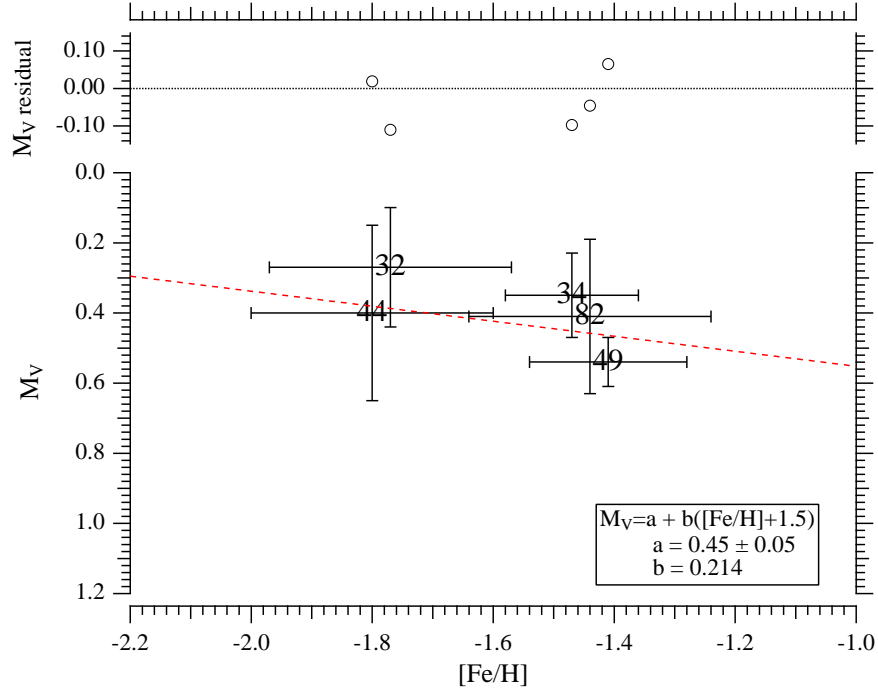


Fig. 7.— RRL extinction-corrected absolute magnitude M_V plotted against metallicity, $[Fe/H]$, whose sources are given in Table 1. Objects are identified by model number: RZ Cep = 32; UV Oct = 34; SU Dra = 44; RR Lyr = 49; XZ Cyg = 82. Errors in M_V and $[Fe/H]$ are $1-\sigma$. The dashed line is an impartial fit to both the absolute magnitude and metallicity data with an adopted slope, $b = 0.214$ (Gratton et al. 2004), resulting in a zero-point, $a = +0.45 \pm 0.05$. The RMS residual to this fit is 0.08 magnitudes.